The Journal of Physiology

Dynamic measurement of the calcium buffering properties of the sarcoplasmic reticulum in mouse skeletal muscle

Carlo Manno[1], Monika Sztretye[2], Lourdes Figueroa[1], Paul D. Allen[3] and Eduardo Ríos[1]

[1] *Section of Cellular Signaling, Department of Molecular Biophysics and Physiology, Rush University, 1750 W. Harrison St, Chicago, IL 60612, USA*
[2] *Department of Physiology, University of Debrecen, P.O. Box 22, Hungary*
[3] *Department of Molecular Biosciences, School of Veterinary Medicine, University of California at Davis, 1 Shields Avenue, Davis, CA 95616*

Key points

- The rise in cytosolic calcium ion concentration that triggers muscle contraction requires release of a large amount of calcium from the cellular store, sarcoplasmic reticulum (SR), where it is stored bound, largely to the protein calsequestrin.
- Binding of calcium by calsequestrin is a complex process, believed to involve changes in protein conformation and aggregation. We want to know to what extent these properties, observed *in vitro*, apply inside cells.
- We measured the calcium buffering power of the SR, defined as the ratio of change in total SR calcium by change in free $[Ca^{2+}]_{SR}$, in muscle cells of wild type or calsequestrin-lacking mice, using two different methods to monitor $[Ca^{2+}]_{SR}$ and deriving changes in total SR calcium content from simultaneous measurements of cytosolic $[Ca^{2+}]$.
- The average buffering power during a large, depleting calcium release event was 157 in the wild type and 40 in the calsequestrin-null mice, suggesting that three-quarters of the calcium released normally comes from the calsequestrin-bound pool.
- The Ca^{2+} buffering ability of the SR is different from that of the equivalent concentration of calsequestrin in aqueous solution, the SR exhibiting greater affinity and cooperativity. We conclude that calsequestrin adopts different properties inside cells.
- SR buffering power depends on the SR Ca^{2+} load and on the rate of its changes, a dependence that could be, at least in part, explained by the unique Ca^{2+} binding properties of calsequestrin.
- This study reveals Ca^{2+} buffering as a highly dynamic process, marking it as both a vulnerable link in diseases that involve loss of control of Ca^{2+} release, and a candidate for further study and intervention.

Abstract The buffering power, *B*, of the sarcoplasmic reticulum (SR), ratio of the changes in total and free $[Ca^{2+}]$, was determined in fast-twitch mouse muscle cells subjected to depleting membrane depolarization. Changes in total SR $[Ca^{2+}]$ were measured integrating Ca^{2+} release flux, determined with a cytosolic $[Ca^{2+}]$ monitor. Free $[Ca^{2+}]_{SR}$ was measured using the cameleon D4cpv-Casq1. In 34 wild-type (WT) cells average *B* during the depolarization (ON phase) was 157 (SEM 26), implying that of 157 ions released, 156 were bound inside the SR. *B* was significantly greater when BAPTA, which increases release flux, was present in the cytosol. *B* was greater early in the pulse – when flux was greatest – than at its end, and greater in the ON than in the OFF. In 29 Casq1-null cells, *B* was 40 (3.6). The difference suggests that 75% of the releasable calcium is normally bound to calsequestrin. In the nulls the difference in *B* between ON and OFF was less than in the WT but still significant. This difference and the associated decay in *B* during the ON were not artifacts of a slow SR monitor, as they were also found in the WT when $[Ca^{2+}]_{SR}$ was tracked with the fast dye fluo-5N. The calcium buffering power, binding capacity and non-linear binding properties of the SR measured here could be accounted for by calsequestrin at the concentration present in mammalian muscle, provided that its properties

DOI: 10.1113/jphysiol.2012.243444

were substantially different from those found in solution. Its affinity should be higher, or K_D lower than the conventionally accepted 1 mM; its cooperativity (n in a Hill fit) should be higher and the stoichiometry of binding should be at the higher end of the values derived in solution. The reduction in B during release might reflect changes in calsequestrin conformation upon calcium loss.

(Received 22 August 2012; accepted after revision 6 November 2012; first published online 12 November 2012)
Corresponding author E. Ríos: Section of Cellular Signaling Department of Molecular Biophysics and Physiology, Rush University School of Medicine, 1750 W. Harrison St, Suite 1279JS, Chicago, IL 60612, USA. Email: erios@rush.edu

Abbreviations *B*, buffering power; BTS, *n*-benzyl-*p*-toluene sulphonamide; Casq, calsequestrin gene and plasmid vector; CDI, Ca^{2+}-dependent inactivation; CPVT, cathecolaminergic polymorphic ventricular tachycardia; D4cpv, D4 circularly permut(at)ed Venus; FDB, flexor digitrorum brevis; FRET, Forster resonant energy transfer; MHS, malignant hyperthermia susceptibility; RyR, ryanodine receptor; SR, sarcoplasmic reticulum; TC, terminal cisternae; WT, wild-type.

Introduction

The signal that unleashes contraction in skeletal muscle requires the release of a large amount of calcium from the sarcoplasmic reticulum (SR) into the cytosol. In mammalian fast twitch muscle fibres, the amount released in association with one action potential is estimated at about 200 μmol l^{-1} of aqueous volume in the cytosol. During physiological tetani, the accumulated release associated with repeated action potentials may reach beyond 1 mmol l^{-1} of cytosol. This calcium comes from a small compartment, about 5% of the volume of the cell (Eisenberg, 1984), where the free [Ca^{2+}] at rest is approximately 0.5 mM (Launikonis *et al.* 2005; Rudolf *et al.* 2006; Sztretye *et al.* 2011*a*; Tang *et al.* 2011). Most of the calcium ions released into the cytosol must therefore have been bound to ligands, rather than free in the SR lumen.

Among the ligands of Ca^{2+} identified in the SR of adult fibres, calsequestrin (MacLennan & Wong, 1971) of isoform 1 (Fliegel *et al.* 1987) is quantitatively the most important (MacLennan *et al.* 1972; Murphy *et al.* 2009; Royer *et al.* 2010).

Calsequestrin is interesting for at least four reasons: first and foremost, because of its central buffering role, which is made possible by its ability to bind Ca^{2+} at between 30 and 80 ions per molecule, and is putatively enhanced by the unique properties of the binding reaction as determined in aqueous solutions (Park *et al.* 2003, 2004; Royer & Ríos 2009; Sánchez *et al.* 2012). Second, calsequestrin is believed to exert some sort of control or modulation of the open–close gating of the ryanodine receptor (RyR) release channels, an idea that originated from the association of inherited diseases of cardiac muscle with mutations of the cardiac calsequestrin isoform 2 (Terentyev *et al.* 2003; Valle *et al.* 2008; Faggioni & Knollmann, 2012), and recently found support in skeletal muscle, with the observation of changes in SR membrane permeability to Ca^{2+} in Casq1-null muscle (Canato *et al.* 2010; Sztretye *et al.* 2011*b*). Additionally, the intriguing stoichiometric association of linear polymers of calsequestrin in the lumen of terminal cisternae with individual RyRs prompted the speculation that these polymers have a diffusional focusing role (MacLennan & Reithmeier, 1998). It is hypothesized that Ca^{2+} ions are adsorbed to calsequestrin, in a manner that allows for rapid longitudinal diffusion along the linear polymers and into the sink constituted by the channel mouth. Finally, alterations in the primary sequence of calsequestrin 2 are linked with cathecolaminergic polymorphic ventricular tachycardia (CPVT), an arrhythmia associated with altered Ca^{2+} control (Priori & Chen, 2011), whereas Casq1-null mice experience an increase in myoplasmic [Ca^{2+}] when exposed to volatile anaesthetics (a condition that has been compared to malignant hyperthermia susceptibility (MHS); Protasi *et al.* 2011; Dainese *et al.* 2009), and a deficit of Ca^{2+} control (MacLennan & Zvaritch, 2011). These two observations suggest symmetry between MHS and CPVT as homologous diseases of Ca^{2+} control, and Casq1 and Casq2 as candidate genes for their respective causation (MacLennan & Chen, 2009).

The titration curves of calsequestrin in solution are complex, suggestive of multiple binding sites with different affinity (Park *et al.* 2004; Sánchez *et al.* 2012). Moreover, there is evidence that binding stages of progressively lower affinity, which are observed as [Ca^{2+}] is increased, are accompanied by progressive polymerization in a stereotyped sequence, as if polymerization was necessary for the existence of these low-affinity sites. The functional advantages of such a mechanism should be evident: calsequestrin would adjust as [Ca^{2+}] increases, providing more binding sites instead of saturating (Park *et al.* 2004; Royer & Ríos, 2009).

If calsequestrin is the dominant buffer in the SR and its unique Ca^{2+} binding properties apply *in situ*, then the Ca^{2+} buffering properties of the organelle should reflect these in some way, perhaps exhibit multistage binding or time-dependent changes; in fact, Pape *et al.* (2007) derived the free Ca^{2+} concentration inside the SR, $[Ca^{2+}]_{SR}$, in frog muscle, from the absorbance of tetramethylmurexide, and produced an SR titration curve with 'cooperativity'

(a value of n greater than 1 in fits with eqn (13)).

Recently it has become possible to measure $[Ca^{2+}]_{SR}$ in mammalian muscle (Rudolf *et al.* 2006; Canato *et al.* 2010; Tang *et al.* 2011; Sztretye *et al.* 2011*a*; Wang *et al.* 2012). By combining the measurement of $[Ca^{2+}]_{SR}$ with that of the changes in total calcium content in the organelle, $[Ca]_{T,SR}$, it is therefore possible to directly evaluate the Ca^{2+} buffering power of mammalian SR. Here we have done this in cells that are made to release Ca^{2+} by depolarizing pulses under voltage control. $[Ca^{2+}]_{SR}$ is derived from the ratiometric signal of the biosensor D4cpv-Casq1, while the changes in $[Ca]_{T,SR}$ are calculated by time integration of Ca^{2+} release flux, derived from the measurement of cytosolic free $[Ca^{2+}]$ in parallel with the changes in $[Ca^{2+}]_{SR}$.

These are dynamic measurements, for which temporal resolution must be as high as possible. Indeed, the large fluxes of Ca^{2+} release associated with sudden depolarization may cause $[Ca^{2+}]_{SR}$ to change substantially in milliseconds (e.g. Canato *et al.* 2010; Sztretye *et al.* 2011*b*). This requirement presents a problem for measuring $[Ca^{2+}]_{SR}$ with D4cpv-Casq1. While the kinetic constants of this sensor have not been measured, the cameleon D1, which has similar structure, has a k_{OFF} of $250\ s^{-1}$ (Palmer *et al.* 2004). If the value of this rate constant was the same for D4cpv-Casq1, and the dissociation constant was $70\ \mu M$, k_{ON} would be $3.6 \times 10^6\ M^{-1}\ s^{-1}$ or about 1000 times less than that of a diffusion-limited reaction (e.g. Wade *et al.* 1998; Zhou & Zhong, 2005). The kinetic limitation, which reflects the major molecular rearrangement in the Förster resonant energy transfer (FRET) mechanism, could be made worse by the presence of calsequestrin fused to the cameleon, or other interactions in the crowded lumen of the SR. For these reasons, and as a control, we carried out additional experiments in which the monitoring of $[Ca^{2+}]_{SR}$ was done using fluo-5N trapped in the SR. The technique, first described by Kabbara & Allen (2001), was applied in the present case with modifications inspired by Ziman *et al.* (2010) and Robin *et al.* (2012).

Methods

Ethical approval

Protocols for animal care, transfection and death of the animals were approved by the Institutional Animal Care and Use Committee of Rush University, and were consistent with their ethical standards.

Transfection of flexor digitrorum brevis (FDB) muscles in adult mice and isolation of single cells

The present results were collected from 135 7- to 12-week-old mice (*Mus musculus*, Black Swiss before 01/07/2010 or Swiss Webster, afterwards). Also used were 37 mice lacking Casq1 (Paolini *et al.* 2007). They were of the C57BL6 strain, raised at Charles River Laboratories (Wilmington, MA, USA) and used at 6–10 weeks of age. Some of the results reported here were obtained by analysis of data collected in an earlier study of permeability (Sztretye *et al.* 2011*b*). In most cases muscles were made to express either the biosensor D4cpv-Casq1 or a variant, D4cpv-δAsp, where the cameleon is fused to a deletion variant of Casq1 (Sztretye *et al.* 2011*a*). The method of transfection, which is adapted from DiFranco *et al.* (2006), was detailed by Sztretye *et al.* (2011*a*). Four to 5 days after injection of plasmid the animals were killed by CO_2 inhalation and FDB muscles were removed for imaging or functional studies. The methods of cell separation were as described by Royer *et al.* (2008), where additional details can be found. Experiments were carried out at 20–22°C in 'external' solution.

Solutions

Concentrations are given in mM: External: 140 TEA-CH_3SO_3, 1 $CaCl_2$, 3.5 $MgCl_2$, 10 Hepes, 1 4-AP, 0.5 $CdCl_2$, 0.3 $LaCl_3$, 0.001 tetrodotoxin (citrate) and 0.05 BTS (*n*-benzyl-*p*-toluene sulphonamide). pH was adjusted to 7.2 with TEA-OH and osmolality to 320 mosmol/kg with TEA methanesulfonate.

Internal solutions (in pipette) were either 'EGTA', 'BAPTA' or '15 mM BAPTA' of composition (in mM): 'EGTA': 110 *N*-methylglucamine, 110 L-glutamic acid, 10 EGTA, 10 Tris, 10 glucose, 5 Na-ATP, 5 phosphocreatine Tris, 0.075 X-rhod 1, 3.56 $CaCl_2$ and 7.4 $MgCl_2$. 'BAPTA': 110 *N*-methylglucamine, 110 L-glutamic acid, 5 BAPTA, 10 Tris, 10 glucose, 5 Na-ATP, 5 phosphocreatine Tris, 0.075 X-rhod 1, 1.81 $CaCl_2$ and 6.96 $MgCl_2$. '15 mM BAPTA': 120 potassium L-glutamate, 15 BAPTA, 10 Trizma, 5 Na-ATP, 5 phosphocreatine Tris, 5.4 CaCl2, 7.19 $MgCl_2$ and 10 glucose. pH was set to 7.2 with NaOH and osmolality to 320 mosmol/kg with *N*-methylglucamine. The amounts of added Ca^{2+} and Mg^{2+} were calculated (for a nominal 1 mM $[Mg^{2+}]$ and 100 nM $[Ca^{2+}]$) using the program Maxchelator, version 2.00 (www.stanford.edu/~cpatton/webmaxc2.htm) and the set of affinity constants contained in its parameter file 'W3'. The near equality of the free $[Ca^{2+}]$ reached in cells with these solutions after at least 30 min of establishing whole-cell patch was verified with ratiometric measurements using indo-1.

Voltage clamp

The whole-cell patch clamp technique follows the implementation of Wang *et al.* (1999), with changes described by Royer *et al.* (2008). The clamped cells

were stable in 'BAPTA', as ascertained by the stability of series resistance, linear capacitance (C_m), charging time constant and holding current. The actual recording of Ca^{2+} transients was started after 15–35 min of stable holding at −80 mV, a time when the concentration of EGTA or BAPTA inside the cell was at a substantial fraction of the solution values, which along with the presence of BTS abolished contractile responses. Command potentials blunted with 0.6 ms duration ramps and linear capacitance compensations were used to avoid saturation of the headstage. Non-linear capacitive ('charge movement') currents obtained by conventional subtraction of scaled controls and baseline correction were integrated to calculate intramembranous charge transfers Q_{ON} and Q_{OFF} as functions of V_m. The dependence of Q_{ON} (V_m) was fitted with the Boltzmann function: $Q_{max}/(1+\exp(-(V_m-V_T)/K))$ to derive amount of mobile charge Q_{max}, transition voltage V_T and limiting logarithmic slope $1/K$. The average values of these parameters were not statistically significantly different from those in our previous works with this technique (Royer *et al.* 2008, 2010).

Simultaneous measurement of cytosolic and SR–lumenal [Ca^{2+}] using a biosensor

In the experiments reported here Ca^{2+} transients and release flux were examined in parallel with $[Ca^{2+}]_{SR}$ largely as described by Sztretye *et al.* (2011*a*,*b*). The cells expressed D4cpv-Casq1 or D4cpv-δAsp in the SR; they were voltage clamped and had the high-affinity, long-wavelength Ca^{2+} monitor X-rhod 1 introduced in the cytosol via the patch pipette. Images $F_j(x,t)$ were obtained in line scan mode. F_1 and F_2 represent fluorescence of D4cpv-Casq1 and D4cpv-δAsp, and F_3 of X-rhod 1. The images were acquired in a laser scanning confocal system (SP2; Leica Microsystems, Exton, PA, USA) equipped with acousto-optical tunable elements that allowed excitation of X-rhod 1 (at 594 nm, with emission collected between 610 and 700 nm) alternating line-by-line with the excitation for D4cpv (at 458 nm, with emission collected between 470 and 510 nm for F_1 and 520 and 580 nm for F_2); therefore, images were effectively simultaneous. At the acquisition frequencies used, the alternate illumination resulted in actual intervals of 2.5–10 ms per line (5 ms per line in most cases) in the individual images. Spatial resolution was 0.24 μm per pixel. Line scanning was always parallel to the fibre axis, at 10–15 μm from the glass coverslip.

After averaging $F_j(x,t)$ over x, to obtain $F_j(t)$, the 'FRET ratio' R was calculated as $(F_2-\text{Background}_2)/(F_1-\text{Background}_1)$. Background_i was measured with lasers off. $[Ca^{2+}]_{SR}$ was calculated from the ratio by a generalization of the equilibrium equation (Sztretye *et al.* 2011*a*)

$$[Ca^{2+}] = \beta K_D \frac{R-R_{min}}{R_{max}-R} + \frac{\beta}{k_{on}}\left(\frac{dR}{dt}\right) \times \frac{R_{max}-R_{min}}{[R_{max}-R+\beta(R-R_{min})](R_{max}-R)} \quad (1)$$

where β is the ratio of values of F_1 in the Ca^{2+}-free and the Ca^{2+}-saturated conditions. The parameter values of R_{min} (0.505), R_{max} (1.74), βK_D (222 μM) and β (0.554) were determined in calibrations *in situ* (Sztretye *et al.* 2011*a*). The value of k_{on} was assumed to be $3.6\times10^6\ M^{-1}\ s^{-1}$ (the value determined in solution at room temperature for cameleon D1; Palmer *et al.* 2004).

Determination of free cytosolic [Ca^{2+}]

Average cytosolic $[Ca^{2+}](t)$ is calculated from averaged X-rhod fluorescence $F(t)$ as

$$[Ca^{2+}]_c(t) = \frac{(F-F_{min})\,k_{off} + dF/dt}{(F_{max}-F)\,k_{on}} \quad (2)$$

F_{max} and F_{min} are derived from eqn (2) applied to the resting condition, in which $[Ca^{2+}]_c(0) \equiv [Ca^{2+}]_R$ is assumed equal to that in the pipette (0.1 μM, an assumption based on results by Royer *et al.* 2010). Equation (2) then becomes $0.1\ \mu M = (F-F_{min})\,K_D/(F_{max}-F)$. Other parameter values are given in Sztretye *et al.* (2011*b*).

The calculation of release flux

Ca^{2+} release flux $\dot{Rel}(t)$ was derived from $[Ca^{2+}]_c(t)$ by the removal method (Melzer *et al.* 1984, 1987), which involves assigning parameter values in a model of the removal of released Ca^{2+}, so that the simulation fits the observed decay of cytosolic Ca simultaneously for several evoked transients. Here the method is made more reliable by the presence of a buffer, EGTA or BAPTA, at such concentrations that the incidence of the endogenous buffers in the removal process becomes almost negligible (González *et al.* 1993).

The removal method – if strictly applied – yields $\dot{Rel}$ records of reliable kinetics but unreliable scale. In other words, even in the simplified situation reached in the presence of high [buffer] the removal model is over-parameterized (Schneider *et al.* 1987; see also Stephenson, 1987). Therefore, and to make the scale of the results comparable across fibres, we used the same values of all parameters, except k_{uptake}, which was set for optimal fit of the evolution of $[Ca^{2+}](t)$. The other parameter values were set as follows: $[Dye]_{total}$, $[EGTA]_{total}$ and $[BAPTA]_{total}$ were set proportionally to the concentrations in the pipette

and an exponential 'entry' function of time, namely

$$[\text{Buffer}](t) = a + ([\text{Buffer}]_{\text{pipette}} - a)(1 - e^{t/\tau}) \quad (3)$$

where a is a small negative constant of convenience and τ equals 37.5 min for BAPTA and 34.8 min for EGTA. These values were adapted from an average estimate of EGTA entry by Schuhmeier & Melzer (2004). The slight difference between time constants of BAPTA and EGTA was calculated assuming inverse proportionality between τ and diffusion coefficient D and inverse proportionality between D and molecular radius, which was calculated from the molecular weight. Additionally, it was found that the inclusion of ~1 mM parvalbumin, reacting with both Ca^{2+} and Mg^{2+}, improved slightly the fit of experimental records by the removal model.

The kinetic constants of EGTA:Ca were $k_{on} = 15\ (\mu M\ s)^{-1}$ and $k_{off} = 7.5\ s^{-1}$ (Schuhmeier & Melzer, 2004; Royer *et al.* 2008). For BAPTA:Ca they were $k_{on} = 1000\ (\mu M\ s)^{-1}$ and $k_{off} = 200\ s^{-1}$ (Wu *et al.* 1996). Parvalbumin concentration was set to 1 mM. Its rate constants with Ca^{2+} were set as $k_{on} = 100\ (\mu M\ s)^{-1}$ and $k_{off} = 1\ s^{-1}$; for Mg^{2+} $k_{on} = 0.03\ (\mu M\ s)^{-1}$ and $k_{off} = 3\ s^{-1}$. The value of k_{uptake}, the proportionality constant linking the rate of pump removal to $[Ca^{2+}]_c$, was allowed to vary among cells for best fit of $[Ca^{2+}]_c(t)$. The best fit k_{uptake} varied in the range of 3.5 to 20 ms^{-1}.

Online Supplementary material illustrates how the removal model fits the Ca^{2+} transients. Additionally, it explores how large changes in the assumed values of the parameters listed above affect the determinations of flux, amount released and calcium buffering power of the SR.

Amount released

From $\dot{Rel}(t)$, the flux that exits through release channels, $\dot{R}_{net}(t)$, quantifying the net flux leaving the SR, is derived by subtraction of the pump removal flux, namely

$$\dot{R}_{net}(t) = \dot{Rel}(t) - k_{uptake}\,[Ca^{2+}]_{cyto}(t) \quad (4)$$

The integral of $\dot{R}_{net}$, from the beginning of the pulse until time t, defines $Rel(t)$, the amount released at time t.

$$Rel(t) \equiv \int_0^t \dot{R}_{net}(u)\,du \quad (5)$$

As the images were acquired at low frequencies, the peak of release flux was blunted. This effect was corrected, for the purpose of tabulating peak values, using empirical factors derived as described by Royer *et al.* (2008). The more slowly varying flux during the so-called quasi-steady phase that follows the peak during a long-lasting depolarization can be measured equally well at different acquisition rates and needs no correction.

The measurement of flux is essentially a calculation of rate of change of total calcium concentration, which is derived from the measured free $[Ca^{2+}]$. Blunting arises because a brief peak rate of change will be underestimated by a low sampling frequency, which can only report the average rate in the sample interval. On the other hand the calculation of amount released, the integral in eqn (5), is numerically a sum of increments, which are well measured, independently of the acquisition frequency. Hence the measure of amount released is not sensitive to the acquisition rate.

SR Ca^{2+} buffering power

Buffering power, B, is defined as $d[Ca]_{T,SR}/d[Ca^{2+}]_{SR}$, the derivative of total with respect to free Ca^{2+} concentration in the SR. Because the change in total concentration is derived from the release flux, which is expressed relative to the volume of aqueous solution in the cytosol, a factor is necessary to express the concentration relative to SR volume:

$$B = \frac{d[Ca]_{T,SR}}{d[Ca^{2+}]_{SR}} \times \left[\frac{\text{mol/l of cytosol}}{\text{mol/l of SR}} \times \frac{0.7\ \text{l of cytosol/l of cell}}{0.055\ \text{l of SR/l of cell}}\right] = d[Ca]_{T,SR}/d[Ca^{2+}]_{SR} \times 12.7 \quad (6)$$

The adjustment factor, 12.7, is the ratio of cytosolic volume (0.7 of cell volume; Baylor *et al.* 1982; Sztretye *et al.* 2011*b*) to SR volume (0.055; Eisenberg, 1984). The values of B averaged during the pulse and afterwards will be represented, respectively, as B_{ON} and B_{OFF}; formally:

$$B_{ON} = \Delta[Ca]_{T,\,SR}/\Delta[Ca^{2+}]SR \times 12.7 \text{ during the ON and}$$
$$B_{OFF} = \Delta[Ca]_{T,\,SR}/\Delta[Ca^{2+}]_{SR} \times 12.7 \text{ during the OFF.} \quad (7)$$

Measurement of SR–lumenal $[Ca^{2+}]$ using fluo-5N

As an alternative to the use of D4cpv-Casq1, the fluo-5N technique (Kabbara & Allen, 2001; Ziman *et al.* 2010; Robin *et al.* 2012) was applied. After enzymatic dissociation with collagenase, FDB cells were loaded for 120 min at room temperature in Tyrode solution containing 10 μM fluo-5N AM. Within 60 min after washout, short cells – averaging 500 μm in length – were transferred to the imaging chamber, where they were voltage clamped with patch pipettes of 0.5–1 MΩ. The internal solution in the pipette was based on glutamate and *N*-methylglucamine and included 15 mM BAPTA in addition to X-rhod 1. Line scan records $F_{fluo}(x,t)$ and $F_{X-rhod}(x,t)$ were obtained line-interleaved, using for fluo -5N excitation at 488 nm with emission collected between 500 and 580 nm, and for X-rhod 1 excitation at 594 nm with emission between 610 and 700 nm.

One concern was the possible contribution of fluorescence of X-rhod 1 to the $F_{fluo}(x,t)$ record. The contribution (namely the fluorescence due to X-rhod collected in the emission range of fluo-5N under 488 nm excitation) should be proportional to the measured F_{X-rhod}. The proportionality factor, $f \approx 0.05$, was determined in measurements in aqueous solutions containing X-rhod 1 alone. Experimental data were then corrected according to the formula

$$F_{fluo}\ \text{corrected} = F_{fluo} - f F_{X-rhod} \quad (8)$$

where the F values are fluorescence intensities after subtraction of a background obtained in the respective emission ranges with excitation lasers off. In actual working conditions this contribution (which is proportional to the concentration of X-rhod) reached a maximum of 10% of F_{fluo}.

$F_{fluo}(x, t)$ corrected according to eqn (8) was averaged over the scan line to produce $F_{fluo}(t)$, and used to derive an approximate $[Ca^{2+}]_{SR}$, calculated as

$$[Ca^{2+}]_{SR} = K_D \frac{(F - F_{min})}{(F_{max} - F)} \quad (9)$$

where F is used instead of $F_{fluo}(t)$. Equation (9) is the same as eqn (2) when the kinetic correction term is neglected.

Equation (9) is derived starting from an expression for total fluorescence of fluo-5N as the sum of a term from dye in the SR and another from other compartments, including cytosol and mitochondria.

$$F = F_{SR} + F_{other} \quad (10)$$

F can be written as

$$F = F_{other} + [CaD]e_{CaD} + (D_T - [CaD])e_D \quad (11)$$

where D_T and [CaD] are concentrations of total and Ca-bound dye in the SR, and e_D and e_{CaD} the molar fluorescence of the dye in its free and bound forms. From eqn (11) it follows that $F_{min} = F_{other} + D_T e_D$, an expression that, for the fluorescein dyes, is approximately equal to F_{other}. In turn

$$[CaD] = D_T \frac{[Ca^{2+}]}{[Ca^{2+}] + K_D} \quad (12)$$

which substituted in eqn (11) yields eqn (9).

A basic tenet of the method is that F_{other} is constant, because the conditions of measurement, which include 15 mM BAPTA in the cytosol, render the dye in cytosol and other compartments effectively insensitive to the calcium fluxes and its fluorescence is unchanged. Therefore, $F_{min} \cong F_{other}$ is assumed to be constant. In the Results it is shown that F_{other} varies, and therefore the assumption provides only a rough approximation.

We set $F_{min} = 0.35F_0$, which is the minimum value found in our experiments. For K_D, two values were used, either 133 μM, from calibrations by Ziman *et al.* 2010, or 400 μM, from calibrations by Zima *et al.* (2010) in cardiac muscle. In each case, F_{max} was set (using eqn (9)) so that resting $[Ca^{2+}]_{SR}$ was equal to the average found using the biosensor (352 μM). Because the actual parameter values of fluo-5N are uncertain we will also show the results in terms of normalized fluorescence, so that consequences can be derived independently of assumptions about dye parameters.

Due to the presence of 15 mM BAPTA in the internal solution, these experiments allowed for accurate measurement of the time course of release flux, net flux and the amount of Ca^{2+} released. As in the experiments with biosensors, these flux measures scale with the concentration of BAPTA, which is estimated from eqn (3) and is not well known. The potential propagation of errors in concentration of the main buffer to the main quantitative measurements is explored in the Supplementary material.

Curve fitting

SR titration data, $[Ca]_{T,SR}$ *vs.* $[Ca^{2+}]_{SR}$, was given a simplified description by fitting the Hill equation

$$[Ca_B] = B_{max} \frac{[Ca^{2+}]^n}{[Ca^{2+}]^n + K_D^n} \quad (13)$$

with free parameters n and K_D. [CaB] represents the concentration of bound Ca^{2+}, and does not assume a specific binding stoichiometry.

Results

SR Ca^{2+} buffering power measured dynamically

The procedure is illustrated in Fig. 1 for a wild-type (WT) cell from a mouse FDB muscle. The mouse paw had been injected 4 days earlier with plasmid coding for the biosensor D4cpv-Casq1, which is expressed exclusively in the SR. Cells were patched with a low-resistance pipette and voltage clamped. The figure shows confocal line scan images of fluorescence of the cytosolic Ca^{2+} monitor X-rhod 1, introduced via the patch pipette (Fig. 1*A*), and the FRET ratio of fluorescences of the sensor (Fig. 1*B*). Line averages of X-rhod 1 fluorescence and FRET ratio are plotted in Fig. 1*C* (red and blue). The analysis of these records is illustrated in Fig. 2. Figure 2*A* shows the release flux, calculated from the cytosolic signal as described (Methods; see also Royer *et al.* 2008). The kinetic features of release flux observed when BAPTA is the main cytosolic buffer have been described before (Sztretye *et al.* 2011*b*); they include an early peak, often followed by a second peak or 'hump'. The flux then rapidly reverts to a low

steady level, which persists until the end of the depolarizing pulse. By integration over time of the net release flux eqn (5), the amount of released Ca^{2+} is derived as a function of time (plotted in Fig. 2*B*). From the FRET ratio $[Ca^{2+}]_{SR}$ is derived and plotted in Fig. 2*C*; note that time is on the vertical axis, increasing down, and concentration is on the horizontal axis.

SR Ca^{2+} buffering power, *B*, is defined in eqn (6). B_{ON} and B_{OFF} represent, respectively, the values of *B* averaged during the pulse and after it (eqn (7)). The advantage of defining *B* differentially (rather than as a ratio of total over free calcium concentrations) is that this definition does not require knowledge of the total content in the SR, a value that cannot readily be measured. What can be measured is the amount of calcium released or, more precisely, the increase in total calcium in the cytosol. Because in the experimental conditions used here the cell is a closed system for calcium and, furthermore, the mitochondria have their contribution to calcium flux minimized, the increase in cytosolic calcium is equal to the decrease in $[Ca]_{T,SR}$. Therefore, according to eqn (6), *B* is equal to the derivative of amount released with respect to change in free $[Ca^{2+}]_{SR}$, with a sign change. (Because $[Ca^{2+}]_{SR}$ and release flux are expressed with reference to different volumes, a factor 12.7 is necessary for *B* to be expressed as a ratio of concentrations in the SR, eqn (6).)

This derivative can be visualized on the plot of amount released *vs.* $[Ca^{2+}]_{SR}$, which is referred to as the 'buffer plot' and presented in Fig. 2*D*. Coloured circles mark in all graphs the beginning and end of the pulse. Several features visible in this example were found in most cells studied. Net flux becomes essentially zero at ~300 ms (or earlier in other cases). Of the amount released in this interval, the initial fast phases, which are essentially over by 50–100 ms, contribute more than two-thirds of the total.

In most cases buffering power is greater during the initial phases, decreasing later. In other words, the buffering plot has negative curvature during the ON. The OFF portion is usually linear and has the same slope found at the end of the ON. A large difference between the average slope during the ON ($-B_{ON}$, slope of chord *a*–*a*) and the OFF ($-B_{OFF}$, slope of line *b*–*b*) is always associated with a large negative curvature; the difference is used below as a convenient measure of the curvature of these noisy records.

Because of the possibility that the calsequestrin fused to the biosensor may contribute significantly to the buffering of Ca^{2+}, and or modify the properties of the biosensor, we carried out additional experiments using the fusion of D4cpv with the variant δAsp of Casq 1, in which 17 C-terminal residues have been deleted (Shin *et al.* 2003). This variant has been shown to have a greatly reduced Ca^{2+} binding capacity and an inability to engage in aggregation changes demonstrated in solution (Park *et al.* 2004). The buffering plots from these experiments, one of which is in Fig. 3*C* (red), were similar to those obtained using D4cpv fused to native calsequestrin, with *B* decreasing during the ON and $B_{ON} > B_{OFF}$.

As observed in earlier work (e.g. Sztretye *et al.* 2011*b*), the presence of BAPTA as main buffer in the cytosol increases the magnitude and alters the kinetics of release flux, presumably by reducing or preventing Ca^{2+}-dependent inactivation (CDI). To explore possible interactions between release kinetics and buffering properties, a group of experiments were carried out with EGTA as main buffer in the pipette. Figure 3*A* presents records of flux (black) and net flux (grey), for a cell monitored with D4cpv-δAsp in the presence of

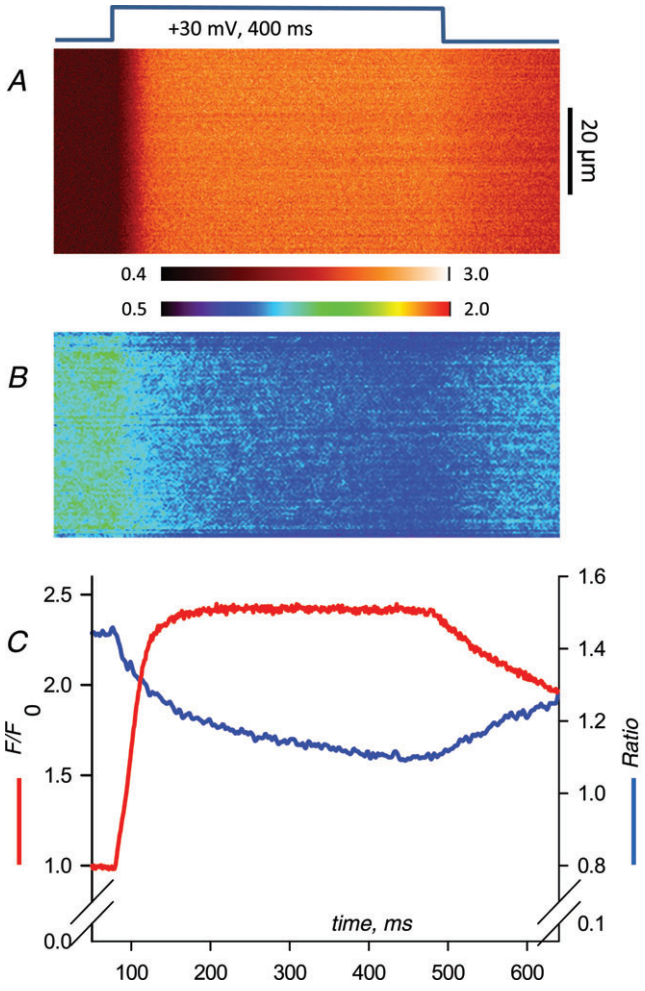

Figure 1. Simultaneous monitoring of cytosolic and SR $[Ca^{2+}]$
An FDB cell expressing D4cpv-Casq1 was whole-cell patched (with X-rhod 1 in the '5 mM BAPTA' perfusing solution), voltage-clamped, held at −80 mV and subjected to the depolarization represented at top. *A*, normalized line scan ($F(x,t)/F_0(x)$) of fluorescence of X-rhod 1. *B*, FRET ratio ($R(x,t)$) of biosensor line scans, simultaneously obtained with the image in *A*. *C*, plot of the line averages of the arrays in *A* and *B*. Identifier: 051209b, series 43. Average of 10 images obtained between 50 and 70 min after whole-cell patching.

10 mM EGTA. Compared with the record in Fig. 2*A*, or with records in Figure 3*B* from a second cell in BAPTA (expressing in this case D4cpv-δAsp), the release flux in the presence of EGTA was lower, presumably because EGTA did not interfere with CDI at the concentrations used. As a consequence, net release flux was positive for a longer time, which required the application of longer pulses to reach maximal depletion in these cells.

The buffering plots of both experiments are shown in Fig. 3*C*. As illustrated, the curvature noted for records in BAPTA is either absent or less pronounced in EGTA; the difference in buffering power between ON and OFF is likewise reduced.

These features are statistically evaluated in Table 1, which presents averages in 34 cells. Twenty-two of these used BAPTA in the internal solution, 14 with D4cpv-Casq1 and 8 withD4cpv-δAsp. Since the δAsp variant introduced no significant differences, results of all the experiments in BAPTA were averaged together. Averages are presented separately for cells in BAPTA and EGTA in the top rows and for both buffers together at the bottom. As already reported, peak flux is significantly greater in BAPTA and the amount released during the pulse is greater in EGTA (Sztretye *et al.* 2011*b*). The table also lists average values of B_{ON} and B_{OFF}. The difference between them is nearly 2-fold and highly significant in BAPTA (or when data in

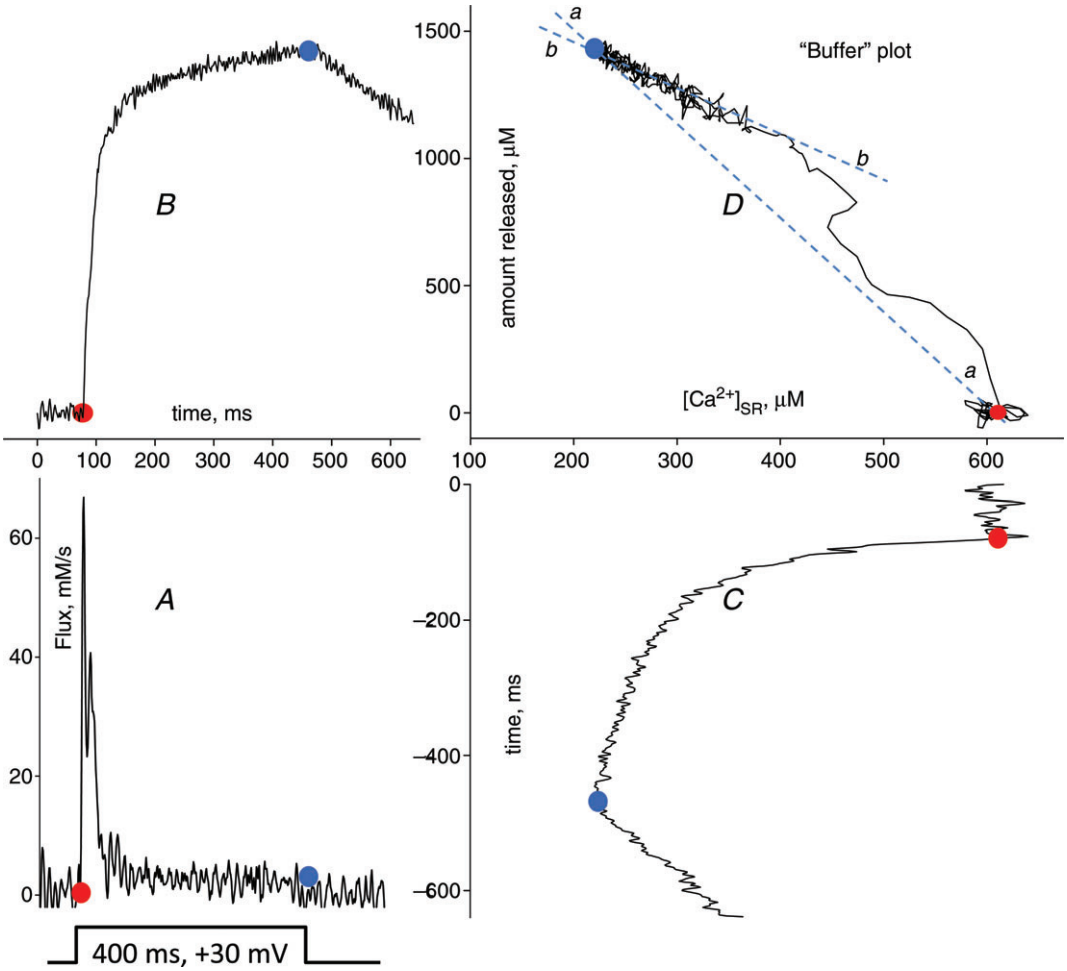

Figure 2. Measurement of buffering power
A, release flux, determined by the standard 'removal' procedure from the record $F(t)/F_0$ in Fig. 1*C*. *B*, the amount released, calculated by time integration of net release flux (see eqn (5)). *C*, the simultaneously measured time course of $[Ca^{2+}]_{SR}$ (derived from the ratio record in Fig. 1*C*). $[Ca^{2+}]_{SR}$ is represented on the abscissa at the top of the panel; time is on the ordinate, incrementing down. *D*, the 'buffer plot', parametric representation of $[Ca^{2+}]_{SR}$ (abscissa) *vs*. amount released. $[Ca^{2+}]_{SR}$ and amount released are represented respectively on the same axes as in *B* and *C*. Coloured circles mark in all panels the beginning and end of the depolarizing pulse. The average buffering power B_{ON} is given by eqn (7) and equals (minus) the slope of the line *a*–*a* traced through the points at the beginning and end of the pulse (further explanation in text). B_{OFF} equals the (minus) slope of the line *b*–*b*, traced through the OFF portion of the plot.

both buffers are averaged together); it is smaller and not significant in EGTA.

This dependence on the nature of the buffer suggests that the curvature is related to the rate at which Ca^{2+} is released, an explanation that also accounts for the greater B_{ON}, as release fluxes are greater than uptake fluxes. A curvature that depends on the rate of release could be an actual property of the SR buffer, but it also could be an artifact. Indeed, if the $[Ca^{2+}]_{SR}$ monitor was too slow to follow the changes the amount released would seem to increase faster than the reported change in $[Ca^{2+}]_{SR}$, and the slope of the $[Ca]_{T,SR}$ *vs.* reported $[Ca^{2+}]_{SR}$ would be greater than the actual *B*.

Such an artifact is a possibility in principle, as the kinetics of the FRET reaction in D4cpv and related cameleons is known to be slow. An OFF rate constant of 250 s^{-1} was reported by Palmer *et al.* (2004) for D1 in solution. This, and a K_D of 90 μM, imply a k_{on} of 2×10^6 M^{-1} s^{-1}, which is three orders of magnitude less than that of diffusion-limited reactions. It should be noted, however, that a reaction with these values of rate constants is still adequate to follow changes with the kinetics observed here, with characteristic times of several milliseconds.

$[Ca^{2+}]_{SR}$ and buffering properties evaluated with fluo-5N

The possibility of an artifact due to slow sensor response was tested by evaluating $[Ca^{2+}]_{SR}$ with a different monitor. Two reasons recommend fluo-5N for this purpose. One is that small synthetic dyes are known to have much faster kinetics than FRET biosensors, thus eliminating the putative artifact. Additionally, given the differential definition used here for buffering power eqns (6) and (7), only the changes in $[Ca^{2+}]_{SR}$ need to be known, rather than the actual $[Ca^{2+}]_{SR}$ values. With this choice, one of the main limitations of non-ratiometric dyes such as fluo-5N, namely the difficulty in obtaining an absolute calibration, is removed.

The use of fluo-5N, introduced by the work of Kabbara & Allen (2001) in an amphibian, is more difficult in mammalian muscle due to the presence of abundant mitochondria close to the SR. Fluo-5N loads into mitochondria and indicates there the increase in $[Ca^{2+}]$ associated with cytosolic Ca^{2+} release. To prevent this signal, Ziman *et al.* (2010) included BAPTA in the cytosol, loaded in AM form, while Robin *et al.* (2012) introduced a high concentration of EGTA (50 mM) via a glass pipette. We tested these and other conditions until finding a procedure that works consistently under patch voltage clamp. Our method consists in loading the cells with fluo-5N AM and using a large patch pipette to diffuse into the cytosol a solution that includes 15 mM BAPTA.

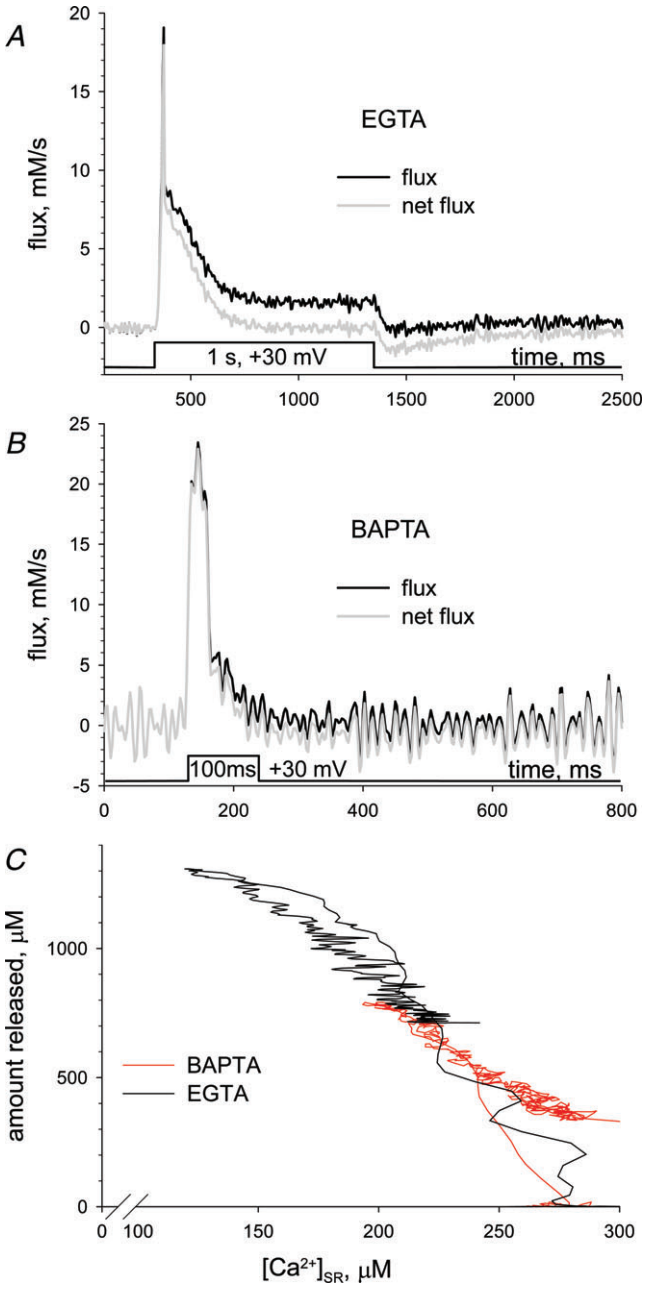

Figure 3. Flux and buffering in cells monitored with D4cpv-δAsp
A, Ca^{2+} release flux (black) and net flux (grey) elicited by a large depolarizing pulse in the presence of 10 mM EGTA in the pipette solution. Identification: 032609c series 34. *B*, corresponding records of flux and net flux in a cell with 5 mM BAPTA in the pipette. Both cells were expressing the D4cpv-δAsp variant of the SR biosensor. Note that net flux remains positive for a much longer time in *A*, which justifies the use of longer lasting pulses in experiments with EGTA. Identification: 012810a series 62. *C*, buffering plots for both cells. No qualitative changes were apparent, but several statistically significant quantitative changes were observed with EGTA, including a smaller curvature of the ON portion of the plot, and a reduction of the difference between ON and OFF slopes. The changes are documented with Table 1.

Table 1. Average buffering properties determined with D4cpv-based biosensors

1	2 Pk flux (mM s^{-1})	3 Amount ON (μM)	4 $[Ca^{2+}]_{SR}$ init (μM)	5 $[Ca^{2+}]_{SR}$ end (μM)	6 $\Delta[Ca^{2+}]_{SR}$ ON (μM)	7 B_{ON}	8 Amount OFF (μM)	9 $[Ca^{2+}]_{SR}$ end OFF (μM)	10 $\Delta[Ca^{2+}]_{SR}$ OFF (μM)	11 B_{OFF}
BAPTA	144[b]	900[b]	352	212	−140[b]	179[a]	−465	350	103	91
($n = 22$)	15	61	49	29	28	36	39	54	28	15
EGTA	63	1568	418	180	−238	101	−765	370	207	78
($n = 12$)	10	180	45	20	30	21	78	66	49	22
All	111	1146[c]	366	197[c]	−169[c]	157[a,c]	−562	356	154[c]	87[c]
($n = 34$)	14	96	37	21	23	26	45	42	25	12

Listed are averages of values found in individual cells, for numbers of cells indicated in the first column. Standard error of the mean is listed immediately below. Columns 2–7 list values corresponding to the ON portion of the response, and corresponding values in the OFF portion are in columns 8–11. Note that both the amount and $\Delta[Ca^{2+}]_{SR}$ change signs between ON and OFF. In column 2 is peak flux. In columns 3 and 8 are amounts (released in column 3, taken up by the SR in column 8), calculated by integration of net flux. In columns 4 and 5 are values of $[Ca^{2+}]_{SR}$ at the beginning and end of the pulse, and in column 6 is their difference, change in $[Ca^{2+}]_{SR}$, during the pulse. Column 9 lists the average concentration at the end of the OFF section of the record, a point of no intrinsic significance (as the OFF restoration of concentrations was incomplete at this time) but for the calculation of $[Ca^{2+}]_{SR}$ increase after depolarization ends. The average of this difference is listed in column 6 for the ON, and column 10 for the OFF. Average buffering power is calculated individually for each fibre as the ratio of the amount released and $\Delta[Ca^{2+}]_{SR}$, then averaged over fibres and changed in sign, to yield the numbers in column 7. A corresponding calculation with OFF values yields the averages in column 11. [a]Significantly greater than corresponding value at the OFF. [b]Significantly different from corresponding value in solution with 10 mM EGTA. [c]Significantly different from corresponding value in the Casq1-null.

As with the biosensor, the fluorescence of fluo-5N was imaged in parallel with that of cytosolic X-rhod 1.

The fluo-5N signal associated with voltage-induced Ca^{2+} release was initially – upon establishing whole-cell patch – an increase of fluorescence during the pulse. It later turned biphasic and became a monotonic decrease after 15 to 20 min of whole-cell patching. Figure 4 shows illustrative line scans of fluorescence of X-rhod 1 and fluo-5N, obtained simultaneously. Line averages of fluorescence during maximal depolarization at different times are shown in Fig. 4*C* and *D*. (To avoid contractile movement, pulses of 1 s or longer were only applied late in the experiment, after a high concentration of BAPTA had been reached in the cytosol.) As shown in Fig. 4*D*, the fluorescence of fluo-5N decays during the pulses, but the extent of the decay increases with time of perfusion.

To derive the buffering properties of the SR, the amount of Ca^{2+} released is calculated in the standard manner (as depicted in Fig. 2) and $[Ca^{2+}]_{SR}$ is derived from the fluo-5N signal. There is considerable uncertainty regarding the calibration of the fluo-5N signals collected in these experiments. As mentioned, in this cell and all others studied similarly, the extent, or amplitude, of the fall in F increased during the experiment. We believe this to be due to the increase in BAPTA concentration, which progressively reduces the contributions to the signal from fluo-5N outside the SR. In the terms introduced with eqn (10), F_{other} is not constant. Consequently, there is no unique value of the parameters F_{min} and F_{max} and therefore $[Ca^{2+}]_{SR}$ cannot be derived rigorously.

The 'shape' of the buffering plot, however, can still be derived. Indeed, the definition of buffering power adopted here requires knowledge of the change in $[Ca^{2+}]_{SR}$, not its actual value. The rapid changes in $[Ca^{2+}]_{SR}$ can still be derived, even though F_{min} and F_{max} vary slowly during the experiment.

The approximate analysis is illustrated in Fig. 5, for the experimental data presented in Fig. 4. Fig. 5*A* plots amount of Ca^{2+} released, calculated from the records in Fig. 4*C*, *vs.* F/F_0 of fluo-5N. Assuming a linear relationship between $[Ca^{2+}]_{SR}$ and F/F_0, this constitutes a first approximation to the buffering plot. That its slope decreases in absolute value during a pulse is in apparent agreement with the observation of negative curvature in the buffering plots derived with the D4cpv-based biosensors. (The comparatively greater noise in these records reflects the use of single images in Figs 4 and 5, whereas Figs 1 and 2 show averaged images and records.)

Linearity, however, is unlikely; the occupancy of the dye by Ca^{2+} at rest should be 50% or greater according to the existing calibrations in skeletal and cardiac muscle cells, which put the K_D at 133 μM (Ziman *et al.* 2010) or 400 μM (Zima *et al.* 2010). Therefore, we abandoned the assumption of linearity, and calculated $[Ca^{2+}]_{SR}$ from F/F_0 using eqn (9) with realistic parameters.

The parameters were derived as follows. F_{min} was made equal to the minimum value observed, 0.35 F_0. F_{max} was calculated solving from eqn (9) in the resting condition. This was done by setting $F = F_0$ and the resting $[Ca^{2+}]_{SR}$ at its average value in the experiments with D4cpv (352 μM).

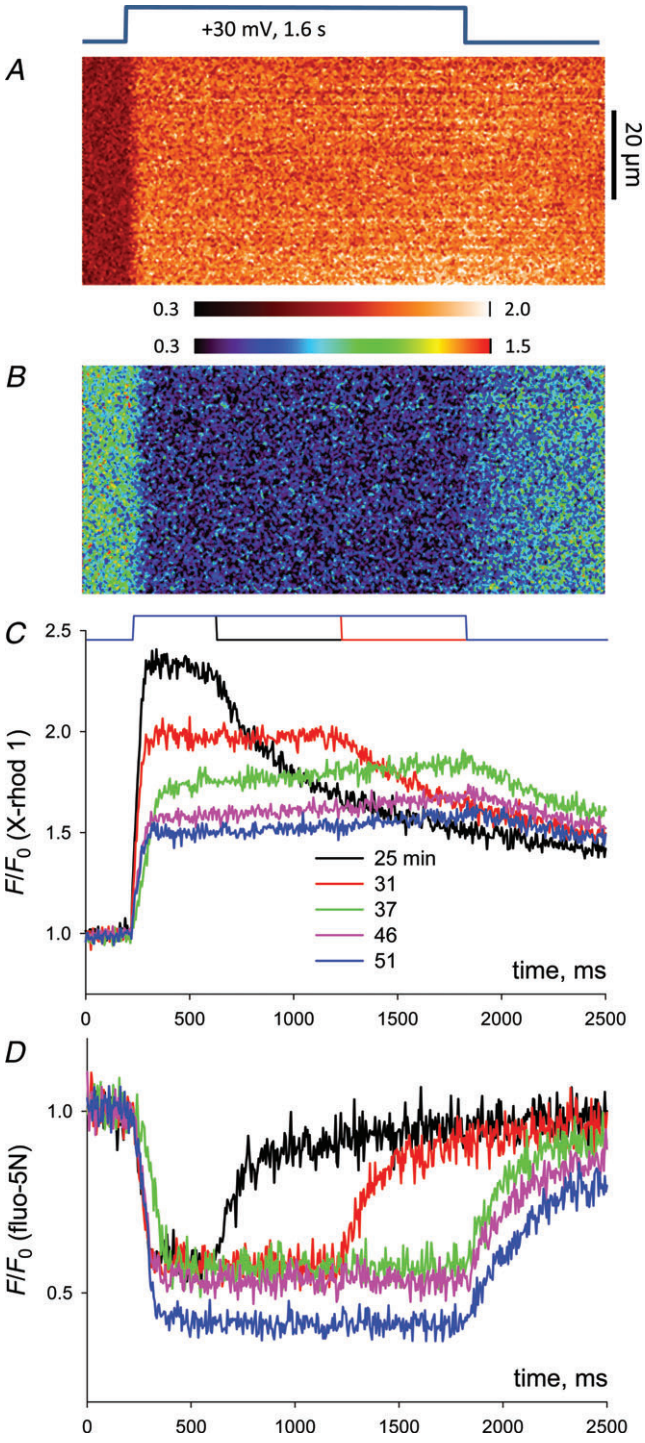

Figure 4. Cytosolic and SR signals in a cell monitored with fluo-5N
An FDB cell was loaded with fluo-5N AM as described in Methods, whole-cell patched (with '15 mM BAPTA' solution in the pipette) and subjected to the large depolarizations represented schematically. *A*, normalized line scan of fluorescence of cytosolic X-rhod 1 acquired while the pulse at top was applied. *B*, normalized line scan of fluorescence of fluo-5N acquired simultaneously with that in *A*. These are individual images obtained 37 min after establishing whole-cell patch. *C* and *D*, line averages of normalized fluorescence for pulses applied at different times (indicated in *C*) during the experiment. The records in green trace correspond to the images in *A* and *B*. Pulses of long duration can only be applied after BAPTA, diffusing from the pipette, reaches a concentration sufficient to prevent movement. The amplitude of the X-rhod 1 signal decays with time, presumably due, at least in part, to the increase in [BAPTA]. The amplitude of the fluo-5N signal increases with time, which suggests a progressive reduction of extra-SR fluorescence. Identification: 042512b, series 78 (*A*, *B*) or 76, 77, 78, 80, 81 (*C*, *D*).

Deriving F_{max} this way required a value of K_D, for which both estimates, 400 and 133 μM, were used.

For the experiment illustrated, the results with $K_D = 400$ and 133 μM are plotted, respectively, in Fig. 5*B* and *C*. As shown, the curvature observed in the raw records is progressively attenuated as K_D is decreased (this is because assuming a lower K_D results in increasing saturation of the dye at rest, which has the effect of magnifying the change in $[Ca^{2+}]_{SR}$ early in the pulse, thus linearizing the buffer plot). A small curvature persists, however, even at the lower K_D. Also as observed with D4cpv-Casq1, the average buffering power B_{ON} remains greater than B_{OFF}. These features are present in the averages, derived from 17 image pairs in five cells, listed in Table 2. Specifically, the difference between B_{ON} and B_{OFF} is approximately a factor of 2 for the case $K_D = 133$ μM. Based on the consistency of the results obtained with both techniques we provisionally conclude that the Ca^{2+} buffering power of the SR decays as $[Ca^{2+}]_{SR}$ decreases. Quantitatively, the decay is such that the buffering power is reduced to ~50% of the average B_{ON} by the end of a long-lasting depleting depolarization.

While the pictures of SR Ca^{2+} buffering properties derived with these two measures of $[Ca^{2+}]_{SR}$ are qualitatively consistent, they show substantial quantitative differences. Most notably, $[Ca^{2+}]_{SR}$ appears to decay (deplete) more in the fluo-5N studies; its average at the end of the depolarizing pulses is 48 μM, while in the D4cpv experiments it is 197 μM. $\Delta[Ca^{2+}]_{SR}$ is consequently greater and *B* smaller in the experiments with fluo-5N. Other differences could be due to fortuitous variation. Thus, in the examples shown, the OFF portion of the buffer plot is curved in the records obtained with fluo-5N, while it is largely linear in the records with D4cpv. The OFF curvature in the fluo-5N plots, however, was not a usual finding; moreover, curved OFF plots were also found in experiments using D4cpv-Casq1, as the next subsection will show.

Buffering properties in cells devoid of calsequestrin

To quantify the contribution by calsequestrin to buffering of Ca^{2+} by the SR we repeated the measurements of Ca^{2+} release flux and $[Ca^{2+}]_{SR}$ in muscle fibres of mice null for Casq1. Figure 6 plots relevant records from two

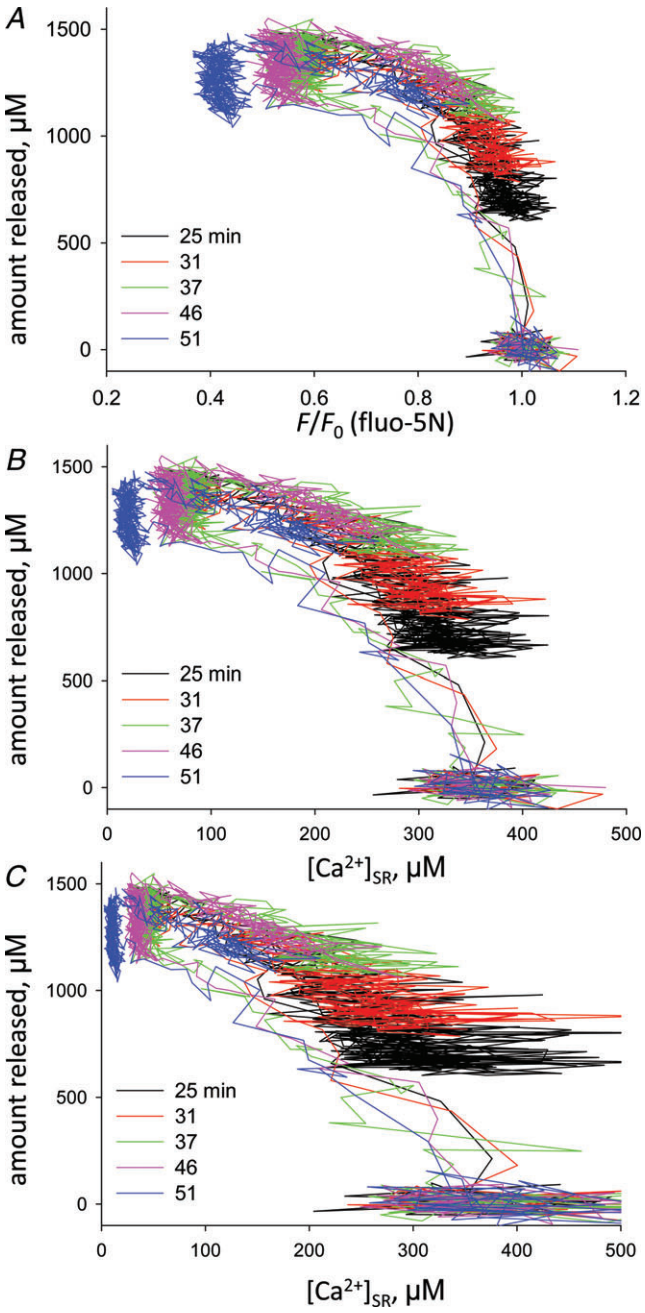

Figure 5. Buffering plots in a cell monitored with fluo-5N
A, normalized fluorescence of fluo-5N, taken directly from the records in Fig. 4, *vs.* amount released, calculated from the corresponding cytosolic calcium transients (X-rhod 1 records in Fig. 4*C*). *B* and *C*, buffering plots derived from the same images, with $[Ca^{2+}]_{SR}$ on the abscissa, calculated with $F_{min}/F_0 = 0.35$, $K_D = 400\ \mu M$ (for *B*) or 133 μM (for *C*) and $F_{max}/F_0 = 1.74$ (*B*) or 1.25 (*C*). These parameter values, which span the results of experimental calibrations, are justified further in the text. Within the range of estimated parameters the buffering plots retain some negative curvature. The plots indicate that a unique set of parameters does not apply strictly for the full course of the experiment, as its use leads to an apparent increase in the degree of depletion (the left-most reach of the plot shifts to the left) in successive applications of the same pulse.

representative cells. Figure 6*A* and *B* present the Ca^{2+} release flux, showing in these and all 29 cells studied a waveform consisting of a single sharp peak that decays during the pulse to a much lower level, which is hardly separable from noise. These kinetics, and specifically the virtual absence of the so-called quasi-steady stage after the initial peak, is a characteristic feature of flux in Casq-null cells (Royer *et al.* 2010; Sztretye *et al.* 2011*b*). In the lower panels are the corresponding buffer plots. In all cases studied these had a slope substantially lower than that typical of WT cells. In the first example (Fig. 6*C*) the slope was fairly constant and about the same during the ON and the OFF. In other cases, illustrated in the second example (Fig. 6*D*), the ON portion of the plot (grey) had marked negative curvature.

Averages are shown in Table 3, separately for cells in the internal solution containing BAPTA or EGTA. Again, approximately half of the experiments with each buffer were done with D4cpv-Casq1 and the others with the D4cpv-δAsp biosensor. The results obtained using the two forms were not significantly different and were pooled for averaging. In 12 of 21 cells studied in BAPTA but only 1 of 8 in EGTA there was visible downward curvature in the buffering plot during the ON. In all these cases the OFF portion of the plot was linear or only slightly curved, and its slope was less (i.e. B_{ON} was greater than B_{OFF}).

B in the null cells was approximately four times smaller than in the WT and the difference was highly significant. The difference between B_{ON} and B_{OFF} was smaller than in the WT, but still significant. Other properties (peak flux, amount released and degree of depletion during a maximal depolarization) were consistent with earlier studies (Royer *et al.* 2010; Sztretye *et al.* 2011*b*). This agreement does not constitute an independent confirmation of the early observations, as approximately half of the cells from which the present data were derived were included (for calculating peak flux, degree of depletion and permeability) in the study by Sztretye *et al.* (2011b).

Discussion

This work combined dynamic measurement of free Ca^{2+} concentration inside the SR by two methods with simultaneous determination of the amount of Ca^{2+} released from the SR, to derive directly the Ca^{2+} buffering properties of the SR. While the present study is a first for mammalian muscle, Pape *et al.* (2007) provided the first estimates of buffering by the SR, using tetramethylmurexide to monitor $[Ca^{2+}]_{SR}$ in the frog.

On cells under voltage clamp we imposed a large, long-lasting depolarization, to cause substantial depletion of the SR. As in prior studies, the presence of a large concentration of an exogenous Ca^{2+} buffer was used to simplify the quantification of released Ca^{2+}. Two buffers

Table 2. Average buffering properties determined with fluo-5N

1	2 Pk flux (mM s^{-1})	3 Amount ON (μM)	4 $[Ca^{2+}]_{SR}$ init (μM)	5 $[Ca^{2+}]_{SR}$ end (μM)	6 $\Delta[Ca^{2+}]_{SR}$ (μM)	7 B_{ON}	8 Amount OFF (μM)	9 $[Ca^{2+}]_{SR}$ end OFF (μM)	10 $\Delta[Ca^{2+}]_{SR}$ OFF (μM)	11 B_{OFF}
Average	126	1358	352	48[b]	−304[b]	57[a,b]	−500	267	219	30[b]
SEM	14	66	n.a.	8	8	2.3	51	19	14	3.4

Averages and SEM are listed in columns numbered as in Table 1. $[Ca^{2+}]_{SR}$ was derived from the fluo-5N signal as described in the text, with $F_{min}/F_0 = 0.35$, $K_D = 133$ μM and $F_{max}/F_0 = 1.74$. Values individually determined in 17 pairs of line scan images in five cells (at 3–5 image pairs per cell) were averaged with equal weight per cell. [a]Significantly greater than corresponding value at the OFF. [b]Significantly different from corresponding value in experiments with D4cpv-based biosensors.

were used alternately, of which EGTA (at the concentration used) is thought not to alter the intrinsic kinetics of release (González and Ríos, 1993), while BAPTA accelerates Ca^{2+} release, presumably by interfering with CDI (Baylor *et al.* 1983; Melzer *et al.* 1984; Pape *et al.* 1995; Pizarro & Ríos, 2004). As in the study by Sztretye *et al.* (2011*b*), these two conditions led to Ca^{2+} release with sharply different time courses.

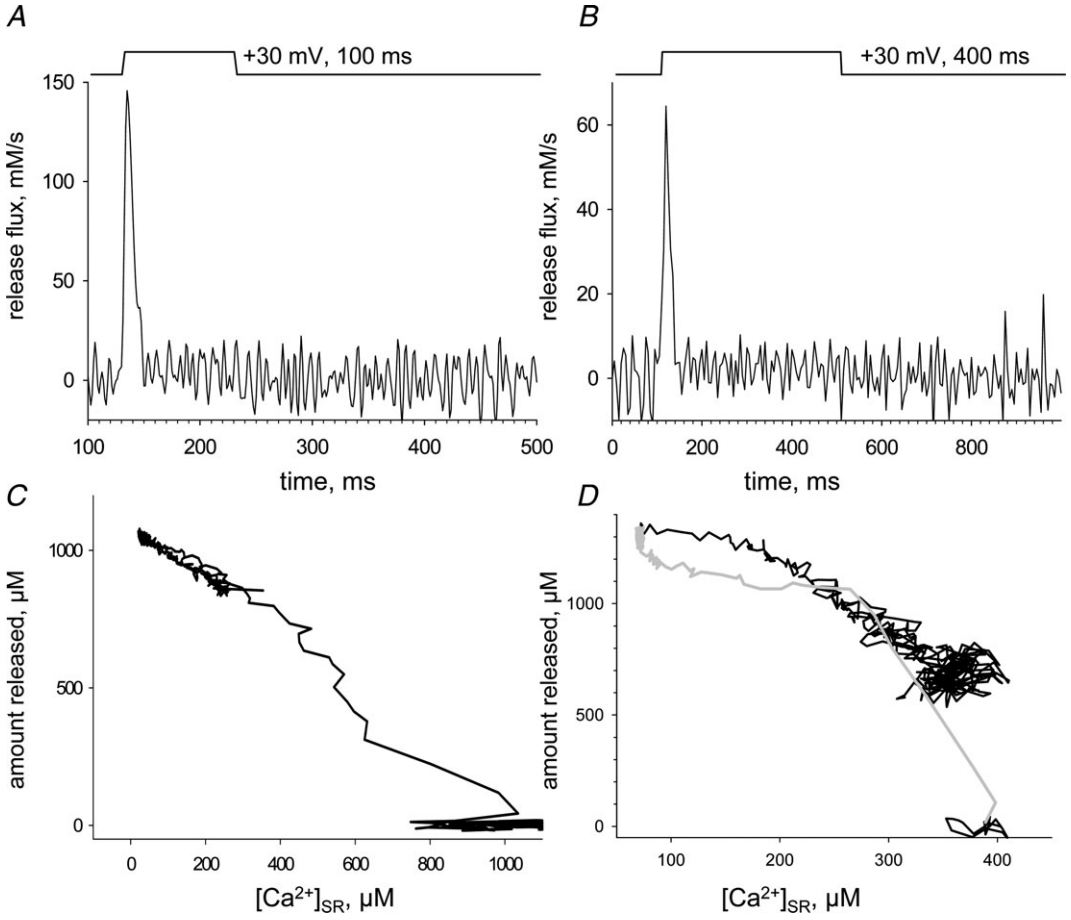

Figure 6. Buffering plots in muscle fibers from Casq1-null mice
FDB cells from null mice were treated as described for Fig. 1 and images processed for derivation of buffer plots as in Fig. 2. *A* and *B*, release flux upon maximal depolarization, recorded in two fibres from different mice, using 5 mM BAPTA internal solution. Both show kinetics characteristic of Casq1-null cells, notable for a sharp decay and lack of a quasi-steady phase. *C* and *D*, corresponding buffer plots. The plot in *C* is approximately linear, with similar slopes during ON and OFF. The plot in *D*, where the ON portion is plotted in grey, exhibits negative curvature, similar to that found in WT cells. A statistical summary of buffering properties of Casq1-null cells is given in Table 3. Identification: *A* and *C*, 08209a series 39; *B* and *D*, 051110a series 10.

Table 3. Buffering properties of Casq1-null cells

1	2 Pk flux (mM s^{-1})	3 Amount ON (μM)	4 $[Ca^{2+}]_{SR}$ init (μM)	5 $[Ca^{2+}]_{SR}$ end (μM)	6 $\Delta[Ca^{2+}]_{SR}$ ON (μM)	7 B_{ON}	8 Amount OFF (μM)	9 $[Ca^{2+}]_{SR}$ end OFF (μM)	10 $\Delta[Ca^{2+}]_{SR}$ OFF (μM)	11 B_{OFF}
BAPTA	132[b]	800	529	102[b]	−399	36[a]	−392	415	347[b]	20[b]
($n = 21$)	26	68	50	18	57	4.5	58	40	44	3.3
EGTA	32	1046	330	36	−294	49	−543	194	159	50
($n = 8$)	5	151	59	8	55	5.8	122	47	41	7.5
All	103	868[c]	474	78[c]	−368[c]	40[a,c]	−434	354	295[c]	28[c]
($n = 29$)	20	66	43	14	44	3.6	54	36	37	4.0

Results were determined with D4cpv-based biosensors in individual fibres, then averaged and listed as described for Table 1. [a]Significantly greater than corresponding value at the OFF. [b]Significantly different from corresponding value in solution with 10 mM EGTA. [c]Significantly different from corresponding value in the wild-type.

Average Ca^{2+} buffering power

The buffering power averaged during a long depolarization was similar with either buffer. Its average over all WT fibres, listed in Table 1, was 157. In other words, during the release process elicited by the large depolarization, for every ion that came from free solution 156 derived from the pool bound inside the SR. (Note that using individually calculated values of buffering power is not the only way to find an average B. Ratioing the average changes in total and free $[Ca^{2+}]_{SR}$ listed in Table 1, the resulting values are smaller (average $B_{ON} = 86$, $B_{OFF} = 46$). That the alternative procedures yield different results is due to a skewed distribution of individual values. Either averaging procedure returns a near 2-fold difference between B_{ON} and B_{OFF}.)

As the slope of the OFF segment of the plot is usually the same as that at the end of the ON portion, a B_{ON} greater than B_{OFF} is always associated with negative curvature (downward concavity) of the buffering plot. The B_{ON} *vs.* B_{OFF} difference is used here as a practical indicator of curvature, which is otherwise difficult to characterize when plots are noisy.

Buffering is reduced in Casq1-null cells

A first evaluation of the role of calsequestrin emerges from the measurement in Casq1-null cells. Comparing entries in Tables 1 and 3, the average B_{ON} of the WT is four times greater than that in the null cells. Based on a number of negative findings in preparations with knockout or knockdown of calsequestrin in skeletal and cardiac preparations (Knollmann *et al.* 2006; Wang *et al.* 2006; Paolini *et al.* 2007; Chopra *et al.* 2007; Meissner *et al.* 2009; Knollmann, 2009) it can be assumed that other buffering molecules remain at the same concentration in the null cells. Under this assumption, a reduction in buffering power by 75% upon deletion of Casq implies that 3 of 4 Ca^{2+} ions released are stored in calsequestrin.

Calsequestrin may account for most Ca^{2+} buffering in the SR

Since the early studies (Ikemoto *et al.* 1972; Oswald & MacLennan, 1974; Aaron *et al.* 1984), the binding properties of calsequestrin 1 were described with the formalism of a conventional 'cooperative' ligand, namely by fits with the Hill equation (eqn (13)). These studies, conducted in the presence of 0.1 mM KCl, yielded values near 1 mM for K_D and $n \approx 2$, a value that suggests positive interaction between two or more binding sites. It was also found that the affinity increased in the absence of K^+ as did the value of n, indicating a complex binding process that includes weak interactions among a multiplicity of relatively non-selective sites. Later studies revealed multiple negatively charged sites on the protein, and showed that its conformation and aggregation state in solution changes as Ca^{2+} binds (reviewed by Royer & Ríos, 2009). The multi-stage binding process is reflected in complex titration curves for which eqn (13) can only provide rough approximations.

To appraise further the contribution of calsequestrin we compare in the following the buffering properties measured here with those found in previous studies of calsequestrin. This is done in two ways, as illustrated in Fig. 7.

In red trace in Fig. 7*A* is an idealization of our average buffering plot (amount released *vs.* $[Ca^{2+}]_{SR}$). Note that the curve starts at the point ($[Ca^{2+}]_{SR} = 366$ μM, amount released $= 0$ μM) and ends at (196, 1146). These are the average values listed in Table 1. The two points are joined by a smooth curve, a cubic polynomial, adjusted to have a slope at the end point (196, 1146) that is approximately half of that of the chord *a*–*a*. The curve is therefore a noise-free representation of average results that includes the mean values of changes in solution and the observed curvature (see first Discussion subsection for detailed values).

These data are used to produce the curve in thick black trace, plot of $[Ca]_{T,SR}$ *vs.* $[Ca^{2+}]_{SR}$, which we will refer to as the 'SR titration curve'. $[Ca]_{T,SR}$ is calculated by

subtracting the amount released (ordinate of the buffering plot in red) from an initial (resting) value. This value is such that after release a small but finite amount remains. This remnant was set to 250 μM in the example, but the choice could have been different without altering the conclusions of the present analysis.

Next we compare this titration curve to model ones, calculated with eqn (13). The curves in green and pink are calculated with the conventional values $K_D = 1$ mM and $n = 2$, and two extreme values for B_{max}. These were calculated as follows: the concentration of calsequestrin is 36 μmol l^{-1} of cell (measured in rat muscle by Murphy *et al.* 2009) or 36/0.7 (=51.4) μmol l^{-1} of cytosolic aqueous solution (Baylor *et al.* 1983; Sztretye *et al.* 2011*b*). B_{max} is therefore 51.4 μM multiplied by the maximal number of Ca^{2+} ions that can bind to one

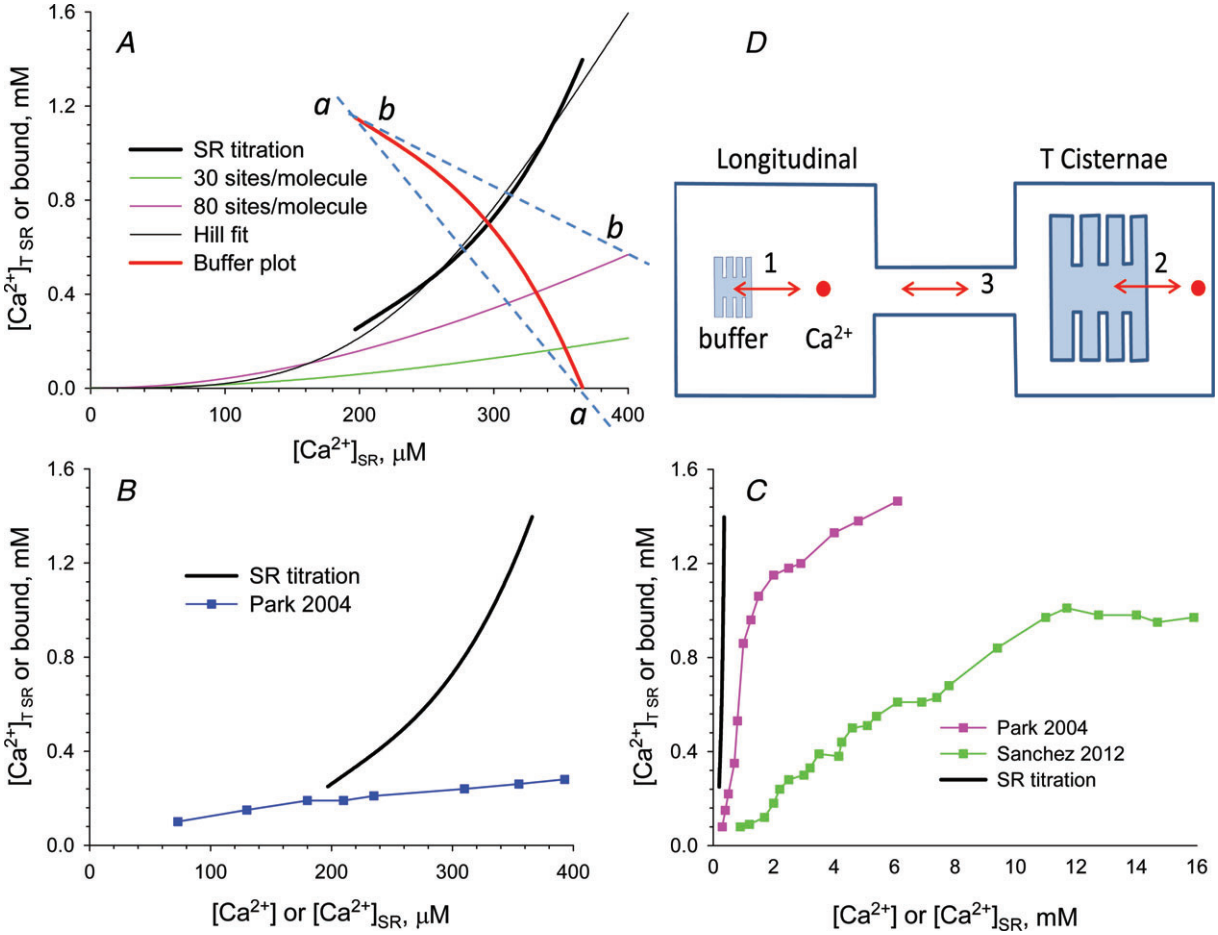

Figure 7. Buffering in the SR compared with titrations of calsequestrin
A, red: idealized buffer plot summarizing experimental measurements in the WT, from averages. The curve, which joins average values, listed in Table 1, at the beginning ($[Ca^{2+}]_{SR} = 366$ μM, amount released = 0) and end of depolarizing pulses ($[Ca^{2+}]_{SR} = 197$ μM, amount released = 1146 μM) is a cubic polynomial fitted to have final slope (indicated by tangent *b*–*b*) equal to 0.5 of that of the chord *a*–*a*. Black, thick trace: SR titration curve ($[Ca]_{T,SR}$ *vs.* $[Ca^{2+}]_{SR}$) derived from the buffer plot as described in the text. Green and pink: bound calcium concentration, calculated with eqn (13), with $K_D = 1$ mM, $n = 2$ and $B_{max} = 1.54$ mM (a number derived as described in the text, assuming that up to 30 Ca^{2+} ions may bind per calsequestrin molecule) or $B_{max} = 4.11$ mM (assuming 80 sites per protein molecule). Black, thin line: fit with eqn (13) to SR titration curve, with B_{max} set at 4.11 mM and best-fit parameters $K_D = 0.46$ mM and $n = 3.52$. *B*, black: SR titration curve from *A*. Blue: titration of purified rabbit calsequestrin in solution, from inset of fig. 5 in Park *et al.* 2004. *C*, SR titration curve (black) compared with two titrations of calsequestrin in solution. Green: titration of recombinant human calsequestrin, redrawn from Sánchez *et al.* 2012. Pink: titration of purified rabbit calsequestrin, redrawn from Park *et al.* (2004). *D*, diagram illustrating the properties of a hypothetical two-compartment organelle, longitudinal SR and TC, assumed to have different buffer concentrations. For this difference to manifest itself in a change in buffering power similar to that found experimentally, the diffusion process (no. 3 in the diagram) connecting the two compartments must have characteristic times of the order of 100 ms and be much slower than the binding reaction in the TC (no. 2). Additionally, the buffer in TC must also have a concentration-dependent buffering power (i.e. changing curvature in its titration).

calsequestrin molecule. The curves used two estimates of this number that span the range found in the literature: 30 (measured by Sánchez *et al.* 2012, with human recombinant calsequestrin1) and 80 (measured by Park *et al.* 2004, with purified rabbit protein). While both models produce plots with the right curvature, neither comes close to the measured bound content in the SR titration curve.

A third attempt to describe our data with the Hill model is represented by the curve in thin black trace. It represents a fit to the data by eqn (13) with freely adjustable n and K_D, and B_{max} set to the greatest of the current estimates ($51.4 \times 80 = 4114\ \mu mol\ l^{-1}$ of cytosol). The best-fit values were $n = 3.52$ and $K_D = 0.46$ mM.

We conclude from these comparisons that the SR Ca^{2+} buffering ability found in the present study may be accounted for by calsequestrin at the concentrations measured by Murphy *et al.* (2009), provided that binding occurred with stoichiometry at the upper end of existing estimates, and with greater affinity and cooperativity than is assumed in current descriptions.

We completed the comparison as illustrated in Fig. 7*B* and *C*, by comparing the SR titration curve (black trace) with two published titrations *in vitro* (Park *et al.* 2004; Sánchez *et al.* 2012). In blue in Fig. 7*B* is our retracing of data at low $[Ca^{2+}]$ of Park *et al.* (2004) (inset of their fig. 5*A*). The data, originally provided as ions per protein molecule, are scaled here by the molar concentration of calsequestrin (51.4 μM). Clearly, Ca^{2+} binding with the properties found *in vitro* by Park *et al.* (2004) does not come close to accounting for the present results. The data of Sánchez *et al.* (2012), which reflect lower binding capacity, are an even worse mismatch, falling outside the 0–400 μM range of the abscissa in Fig. 7*B*.

To better demonstrate the discrepancy we plotted in Fig. 7*C* the two titrations *in vitro* and our SR titration curve on a greatly compressed $[Ca^{2+}]_{SR}$ scale. Our titration curve is again plotted in black. The mismatch is enormous; while the binding capacity measured *in vitro* may be consistent with that of the SR, buffering in the SR is much more powerful – the slope is much greater – and the organelle is capable of storing large quantities of bound Ca^{2+} at free Ca^{2+} concentrations that cause negligible binding to calsequestrin *in vitro*. It is also remarkable that the binding curves *in vitro* do not display the curvature observed in our SR titration.

Murphy *et al.* (2009), who noted the discrepancy, suggested as an explanation the presence of KCl at the un-physiologically high concentration of 0.3 M in the *in vitro* measurements. While it is unlikely that a 2- or 3-fold change in the concentration of potassium will change the effective affinity by orders of magnitude, the presence of chloride at a concentration approximately 30-fold higher than in the myoplasm could account for some of the difference.

The conclusion from these comparisons is that calsequestrin, at the concentrations measured by Murphy *et al.* (2009) and having binding capacity somewhere between 30 and 80 ions per molecule, may account for the releasable Ca^{2+} in the present study only if its affinity is increased severalfold compared with that observed *in vitro*, and the binding features that determine the effective cooperativity are changed as well. Echoing a suggestion by ChulHee Kang (personal communication) we suggest that within the highly crowded and structured environment of a working SR, and due to interactions that cannot be recreated *in vitro*, the protein adopts conformations that are optimal for buffering of calcium.

The curvature in SR Ca^{2+} titration

Model titrations with positive curvature can be derived with eqn (13) and $n > 1$, but as shown with Fig. 7*A* even using $n = 3.52$ the curvature in the fit is less than that observed experimentally. As the curvature was lower in the buffering plots of Casq1-null cells, it appears that the high curvature is a property of Ca^{2+} binding to calsequestrin.

An intriguing feature of the observations is that the curvature is greater when BAPTA is present in the cytosol (which leads to faster transients) and is greater in the ON (when changes are faster) than the OFF. It therefore appears that fast changes in lumenal Ca^{2+} concentrations, of free or bound ions, enhance the curvature.

This dependence will arise trivially if the $[Ca^{2+}]_{SR}$ sensor is slow, so that its signal lags the actual $[Ca^{2+}]_{SR}$ change. In this hypothesis the change in $[Ca]_{T,SR}$, evaluated with a faster dye in the cytosol, will seem faster, and the buffering power will appear to be higher early during the pulse, when flux is greatest. This simple explanation was rejected on the basis of measurements of $[Ca^{2+}]_{SR}$ with a second monitor, the small synthetic dye fluo-5N, which by analogy with other fluorescein-based dyes is believed to have a much greater k_{on} (e.g. Eberhard & Erne, 1989, for calibrations in solution; Shirokova *et al.* 1996, for calibrations inside cells). In spite of difficulties of calibration, expected for a non-ratiometric monitor, the buffering plots obtained with this dye largely confirmed both the observation of curvature and its magnitude (quantified by the difference between average buffering power during ON and OFF).

A curvature in the buffer plot could also arise as an artifact of erroneous calculation of the amount released. This putative explanation has the virtue of justifying curvature observed with both sensors of SR calcium. The hypothesis was explored and essentially ruled out carrying out a number of alternative calculations of $\dot{R}el(t)$, illustrated in the Supplementary material, using different values for the fixed parameters of the removal model. As stated in Methods and initially established by

Schneider *et al.* (1987), different sets of parameter values, especially different concentrations of the main buffer, result in waveforms of flux that scale proportionally, without otherwise changing their temporal dependence. Consequently, the amount released also scales linearly and, as the Supplementary material demonstrates, the buffer plots maintain the changes in slope – the curvature – even as they shrink or expand vertically.

It seems clear therefore that B (slope of the buffering plot) decreases as SR content is depleted. This change in slope in turn seems to depend on the rate of the change in content, namely the release flux. One possible explanation of this phenomenon is that rapid changes in occupancy of binding sites on calsequestrin destabilize its structure (as suggested by Park *et al.* 2004), leading to depolymerization and decrease in binding capacity and affinity. Furthermore, the alteration would not be immediately reversed, and recovery of $[Ca^{2+}]_{SR}$ in the OFF would proceed with the binding properties reached at the end of the ON stage, precisely as observed. This explanation, however, does not fully account for the data, because some curvature persists in Casq-null cells. That cells devoid of calsequestrin still have a curved SR titration indicates the existence of additional, more general reasons for the observation.

One possibility, suggested by putative observations of Ca^{2+} movements inside the SR (Winegrad, 1965), is that the initial phases of release rely on Ca^{2+} stored in the terminal cisternae, where calsequestrin is located and buffering power is greatest, while release in later stages might rely on Ca^{2+} stored in other regions of the SR and would therefore proceed at a lower buffering power.

This hypothesis is represented in its simplest version in Fig. 7*D* by two compartments (longitudinal SR and terminal cisternae (TC)) of different buffering power connected by diffusion of free Ca^{2+}. The overall B in the release process will reflect initially the high buffering power of TC, provided that reaction in TC (no. 2) is fast compared with diffusional equilibration (no. 3). Later, with TC largely depleted, B will be low, but only if the titration curve of TC has high curvature (in other words, curvature in the primary buffer titration must still be assumed). Substantial differences in concentration develop between the compartments of this model during release.

While the work of Winegrad (1965) was indicative of $[Ca^{2+}]$ gradients and time lags due to intra-SR diffusion, later observations did not support the original observations or the existence of substantial barriers to diffusion. The characteristic time of diffusional equilibration between longitudinal SR and TC in skeletal muscle is estimated at a few milliseconds (see for instance Pape *et al.* 2007), consistent with the ample and unrestricted connections visible in electron micrographs (Franzini-Armstrong, 1964). The change in B reported here develops during depolarizing pulses of 100 ms or more. In 100 ms longitudinal SR and TC would be essentially equilibrated and their contributions would not be separable. Therefore, a 'delayed equilibration' hypothesis does not help understand the non-linearity in SR Ca^{2+} titration.

Two monitors of $[Ca^{2+}]_{SR}$ compared

The present study allows for a direct comparison of two techniques for imaging $[Ca^{2+}]_{SR}$ in muscle fibres treated similarly.

The advantages of D4cpv-Casq1 over the small synthetic dye are 2-fold: D4cpv and FRET sensors are ratiometric, and hence their calibration is straightforward in principle. Additionally, D4cpv-Casq1 expresses only inside the SR, which minimizes interferences from outside the organelle.

These interferences constitute the principal problem for calibrating and interpreting the fluo-5N signal. They are minimized by placing a large amount of buffer in the cytosol, which reduces the fluorescence from dye in both cytosol and mitochondria. As the effect depends on buffer diffusing into the cell, it is progressive, resulting in variation of F_{min} and F_{max} during the experiment. A steady value of these parameters is expected when the buffer concentration is high enough that further increase does not cause additional change in the extra-SR fluorescence, but this point was not clearly reached in our experiments. An additional disadvantage is the requirement of a very high concentration of buffer, 15 mM BAPTA in our case, 50 mM EGTA in the implementation by Robin *et al.* (2012). These concentrations will interfere with physiological release, changing its kinetics. By contrast, the presence of a high concentration of buffer is not required by the biosensor technique. In our implementation, a high buffer concentration is used, but only to measure release flux more accurately.

Fluo-5N and small synthetic dyes in general have two major advantages. One is fast kinetics, with ON rate constants greater by orders of magnitude than those of FRET biosensors *in vitro*. Because of crowding, compounded with the presence of targeting moieties – calsequestrin in the present case – the kinetics of the biosensor could be slowed further inside the SR lumen. It was therefore reassuring that the signals obtained with the two methods were not substantially different, and indicative that the biosensor is sufficiently rapid to follow the $[Ca^{2+}]_{SR}$ changes evoked in this study.

An additional advantage of the fluorescein-based monitors is their dynamic range, which is much greater than that of cameleons and other FRET sensors when compared in aqueous solutions. This advantage, however, is substantially reduced when fluo-5N is applied in cells. Indeed, the dynamic range (defined as F_{max}/F_{min}), which is approximately 200 in dye solutions, was reduced to

approximately 6 in the present experiments (due to contributions to F_{min} by extra-SR compartments; see eqn (10)). The corresponding figure of merit for the biosensor, R_{max}/R_{min}, is 1.75/0.505, or approximately 3.5.

The biosensor has its own shortcomings, including the variability of expression density and some variability in performance, which was accounted for in earlier work as a variance in its parameter values (Sztretye *et al.* 2011*a*).

A problem with both monitors is their affinity for calcium; because their K_D is low by comparison with resting $[Ca^{2+}]_{SR}$, both sensors provide highly non-linear representations of $[Ca^{2+}]$. Signals from a monitor of higher K_D, like the recently described CatchER (Tang *et al.* 2011; Wang *et al.* 2012), contain more easily interpretable information even if their dynamic range and sensitivity are lower.

In summary, D4cpv-Casq1 provides a reliable calibrated signal, while fluo-5N, with its greater sensitivity and speed of response, is a better choice for following rapid changes. A major disadvantage of fluo-5N is the requirement of highly interfering concentrations of buffers in the cytosol. Both sensors have adequate sensitivity for most purposes, but their affinity is excessive for monitoring lumenal SR calcium concentrations.

Conclusions

It is possible to follow the rapid changes in $[Ca^{2+}]_{SR}$ associated with rapid release of Ca^{2+} using either the D4cpv-Casq1 biosensor or fluo-5N, methods that have complementary advantages and shortcomings. Combining these with a cytosolic $[Ca^{2+}]$ monitor we produced a direct measure of SR Ca^{2+} buffering power and a titration of SR Ca^{2+}. The measured buffering power was reduced by 75% in calsequestrin-null muscle, which indicates that calsequestrin contributes 75% of the Ca^{2+} released in the WT. To account for a contribution of this magnitude, calsequestrin at the concentrations measured in muscle must have much greater affinity than it does in solution, and its detailed concentration dependence of binding must change in other ways. Some of the buffering properties depend on the rate of change of SR load, perhaps reflecting time-dependent changes in the dense polymeric network that calsequestrin forms inside the SR. This study reveals Ca^{2+} buffering as a highly dynamic process, which depends on concentration and changes with time. These features mark Ca^{2+} buffering as both a vulnerable link in diseases that involve loss of control of Ca^{2+} release, and a candidate for further study and intervention.

References

Aaron BM, Oikawa K, Reithmeier RA & Sykes BD (1984). Characterization of skeletal muscle calsequestrin by ^{1}H NMR spectroscopy. *J Biol Chem* **259**, 11876–11881.

Baylor SM, Chandler WK & Marshall MW (1982). Use of metallochromic dyes to measure changes in myoplasmic calcium during activity in frog skeletal muscle fibres. *J Physiol* **331**, 139–177.

Baylor SM, Chandler WK & Marshall MW (1983). Sarcoplasmic reticulum calcium release in frog skeletal muscle fibres estimated from Arsenazo III calcium transients. *J Physiol* **344**, 625–666.

Canato M, Scorzeto M, Giacomello M, Protasi F, Reggiani C &Stienen GJ (2010). Massive alterations of sarcoplasmic reticulum free calcium in skeletal muscle fibers lacking calsequestrin revealed by a genetically encoded probe. *Proc Natl Acad Sci U S A* **107**, 22326–22331.

Chopra N, Kannankeril PJ, Yang T, Hlaing T, Holinstat I, Ettensohn K, Pfeifer K, Akin B, Jones LR, Franzini-Armstrong C & Knollmann BC (2007). Modest reductions of cardiac calsequestrin increase sarcoplasmic reticulum Ca^{2+} leak independent of luminal Ca^{2+} and trigger ventricular arrhythmias in mice. *Circ Res* **101**, 617–626.

Dainese M, Quarta M, Lyfenko AD, Paolini C, Canato M, Reggiani C, Dirksen RT & Protasi F (2009). Anesthetic- and heat-induced sudden death in calsequestrin-1-knockout mice. *FASEB J* **23**, 1710–1720.

DiFranco M, Neco P, Capote J, Meera P & Vergara JL (2006). Quantitative evaluation of mammalian skeletal muscle as a heterologous protein expression system. *Protein Expr Purif* **47**, 281–288.

Eberhard M & Erne P (1989). Kinetics of calcium binding to fluo-3 determined by stopped-flow fluorescence. *Biochem Biophys Res Commun.* **163**, 309–314.

Eisenberg BR (1984). Quantitative ultrastructure of mammalian skeletal muscle. In *Handbook of Physiology:* section 10, *Skeletal Muscle*, ed. Peachey LD, pp. 73–112. Williams & Wilkins, Baltimore.

Faggioni M & Knollmann BC (2012). Calsequestrin 2 and arrhythmias. *Am J Physiol Heart Circ Physiol* **302**, H1250–H1260.

Fliegel L, Ohnishi M, Carpenter MR, Khanna VK, Reithmeier RA & MacLennan DH (1987). Amino acid sequence of rabbit fast-twitch skeletal muscle calsequestrin deduced from cDNA and peptide sequencing. *Proc Natl Acad Sci U S A* **84**, 1167–1171.

Franzini-Armstrong C (1964). Fine structure of sarcoplasmic reticulum and transverse tubular system in muscle fibers. *Fed Proc* **23**, 887–895.

González A, Ríos E. 1993. Perchlorate enhances transmission in skeletal muscle excitation-contraction coupling. *J Gen Physiol.* **102:** 373–421.

Ikemoto N, Bhatnagar GM, Nagy B & Gergely J (1972). Interaction of divalent cations with the 55,000-dalton protein component of the sarcoplasmic reticulum. Studies of fluorescence and circular dichroism. *J Biol Chem* **247**, 7835–7837.

Kabbara AA & Allen PD (2001). The use of the indicator fluo-5N to measure sarcoplasmic reticulum calcium in single muscle fibres of the cane toad. *J Physiol* **534**, 87–97.

Knollmann BC, Chopra N, Hlaing T, Akin B, Yang T, Ettensohn K, Knollmann BE, Horton KD, Weissman NJ, Holinstat I, Zhang W, Roden DM, Jones LR, Franzini-Armstrong C & Pfeifer K (2006). Casq2 deletion causes sarcoplasmic reticulum volume increase, premature Ca^{2+} release, and catecholaminergic polymorphic ventricular tachycardia. *J Clin Invest* **116**, 2510–2520.

Knollmann BC (2009). New roles of calsequestrin and triadin in cardiac muscle. *J Physiol* **587**, 3081–3087.

Launikonis BS, Zhou J, Royer L, Shannon TR, Brum G & Ríos E (2005). Confocal imaging of $[Ca^{2+}]$ in cellular organelles by SEER, shifted excitation and emission rationing of fluorescence. *J Physiol* **567**, 523–543.

MacLennan DH & Wong PT (1971). Isolation of a calcium-sequestering protein from sarcoplasmic reticulum. *Proc Natl Acad Sci U S A* **68**, 1231–1235.

MacLennan DH, Yip CC, Iles GH & Seeman P (1972). Isolation of sarcoplasmic reticulum proteins. *Cold Spring Harbor Symp Quant Biol* **37**, 469–478.

MacLennan DH & Reithmeier RA (1998). Ion tamers. *Nat Struct Biol* **5**, 409–441.

MacLennan DH & Chen SR (2009). Store overload-induced Ca^{2+} release as a triggering mechanism for CPVT and MH episodes caused by mutations in *RYR* and *CASQ* genes. *J Physiol* **587**, 3113–3115.

MacLennan DH & Zvaritch E (2011). Mechanistic models for muscle diseases and disorders originating in the sarcoplasmic reticulum. *Biochem Biophys Acta* **1813**, 948–964.

Meissner G, Wang Y, Xu L & Eu JP (2009). Silencing genes of sarcoplasmic reticulum proteins clarifies their roles in excitation–contraction coupling. *J Physiol* **587**, 3089–3090.

Melzer W, Ríos E & Schneider MF (1984). Time course of calcium release and removal in skeletal muscle fibers. *Biophys J* **45**, 637–641.

Melzer W, Ríos E & Schneider MF (1987). A general procedure for determining the rate of calcium release from the sarcoplasmic reticulum in skeletal muscle fibers. *Biophys J* **51**, 849–863.

Murphy RM, Larkins NT, Mollica JP, Beard NA & Lamb GD (2009). Calsequestrin content and SERCA determine normal and maximal Ca^{2+} storage levels in sarcoplasmic reticulum of fast- and slow-twitch fibres of rat. *J Physiol* **587**, 443–460.

Ostwald TJ & MacLennan DH (1974). Isolation of a high affinity calcium-binding protein from sarcoplasmic reticulum. *J Biol Chem* **249**, 974–979.

Palmer AE, Jin C, Reed JC (2004). Tsien RY.Bcl-2-mediated alterations in endoplasmic reticulum Ca2+ analyzed with an improved genetically encoded fluorescent sensor. *Proc Natl Acad Sci USA*. **101:** 17404–9.

Paolini C, Quarta M, Nori A, Boncompagni S, Canato M, Volpe P, Allen PD, Reggiani C & Protasi F (2007). Reorganized stores and impaired calcium handling in skeletal muscle of mice lacking calsequestrin-1. *J Physiol* **583**, 767–784.

Pape PC, Jong DS & Chandler WK (1995). Calcium release and its voltage dependence in frog cut muscle fibers equilibrated with 20 mM EGTA. *J Gen Physiol* **106**, 259–336.

Pape PC, Fénelon K, Lamboley CRH & Stachura D (2007). Role of calsequestrin evaluated from changes in free and total calcium concentrations in the sarcoplasmic reticulum of frog cut skeletal muscle fibres. *J Physiol* **581**, 319–367.

Park H, Wu S, Dunker AK & Kang C (2003). Polymerization of calsequestrin. Implications for Ca^{2+} regulation. *J Biol Chem* **278**, 16176–16182.

Park H, Park IY, Kim E, Youn B, Fields K, Dunker AK & Kang C (2004). Comparing skeletal and cardiac calsequestrin structures and their calcium binding: a proposed mechanism for coupled calcium binding and protein polymerization. *J Biol Chem* **279**, 18026–18033.

Pizarro G & Ríos E (2004). How source content determines intracellular Ca^{2+} release kinetics. Simultaneous measurement of $[Ca^{2+}]$ transients and [H+] displacement in skeletal muscle. *J Gen Physiol* **124**, 239–258.

Priori SG & Chen SR (2011). Inherited dysfunction of sarcoplasmic reticulum Ca^{2+} handling and arrhythmogenesis. *Circ Res* **108**, 871–883.

Protasi F, Paolini C, Canato M, Reggiani C &Quarta M (2011). Lessons from calsequestrin-1 ablation *in vivo*: much more than a Ca^{2+} buffer after all. *J Muscle Res Cell Motil* **32**, 257–270.

Robin G, Berthier C & Allard B (2012). Sarcoplasmic reticulum Ca^{2+} permeation explored from the lumen side in *mdx* muscle fibers under voltage control. *J Gen Physiol* **139**, 209–218.

Royer L, Pouvreau S & Ríos E (2008). Evolution and modulation of intracellular calcium release during long-lasting depleting depolarization in mouse muscle. *J Physiol* **586**, 4609–4629.

Royer L & Ríos E (2009). Deconstructing calsequestrin. Complex buffering in the calcium store of skeletal muscle. *J Physiol* **587**, 3101–3111.

Royer L, Sztretye M, Manno C, Pouvreau S, Zhou J, Knollmann BC, Protasi F, Allen PD & Ríos E (2010). Paradoxical buffering of calcium by calsequestrin demonstrated for the calcium store of skeletal muscle. *J Gen Physiol* **136**, 325–338.

Rudolf R, Magalhães PJ & Pozzan T (2006). Direct *in vivo* monitoring of sarcoplasmic reticulum Ca^{2+} and cytosolic cAMP dynamics in mouse skeletal muscle. *J Cell Biol* **173**, 187–193.

Sánchez EJ, Lewis KM, Danna BR & Kang C (2012). High-capacity Ca^{2+} binding of human skeletal calsequestrin. *J Biol Chem* **287**, 11592–11601.

Schneider MF, Ríos E & Melzer W (1987). Determining the rate of calcium release from the sarcoplasmic reticulum in muscle fibers. *Biophys J* **51**, 1005–1007.

Schuhmeier RP & Melzer W (2004). Voltage-dependent Ca^{2+} fluxes in skeletal myotubes determined using a removal model analysis. *J Gen Physiol* **123**, 33–51.

Shin DW, Pan Z, Kim EK, Lee JM, Bhat MB, Parness J, Kim DH & Ma J (2003). A retrograde signal from calsequestrin for the regulation of store-operated Ca^{2+} entry in skeletal muscle. *J Biol Chem* **31**, 3286–3292.

Shirokova N, García J, Pizarro G & Ríos E (1996). Ca^{2+} release from the sarcoplasmic reticulum compared in amphibian and mammalian skeletal muscle. *J Gen Physiol* **107**, 1–18.

Stephenson DG (1987). Calcium release from the sarcoplasmic reticulum. *Biophys J*. **51**, 1009–1010.

Sztretye M, Yi J, Figueroa L, Zhou J, Royer L & Ríos E (2011a). D4cpv-calsequestrin: a sensitive ratiometric biosensor targeted to the calcium store of skeletal muscle. *J Gen Physiol* **138**, 211–229.

Sztretye M, Yi J, Figueroa L, Zhou J, Royer L, Allen PD, Brum G & Ríos E (2011b). Measurement of RyR permeability reveals a role of calsequestrin in termination of SR Ca^{2+} release in skeletal muscle. *J Gen Physiol* **138**, 231–247.

Tang S, Wong HC, Wang ZM, Huang Y, Zou J, Zhuo Y, Pennati A, Gadda G, Delbono O & Yang JJ (2011). Design and application of a class of sensors to monitor Ca^{2+} dynamics in high Ca^{2+} concentration cellular compartments. *Proc Natl Acad Sci U S A* **108**, 16265–16270.

Terentyev D, Viatchenko-Karpinski S, Györke I, Volpe P, Williams SC & Györke S (2003). Calsequestrin determines the functional size and stability of cardiac intracellular calcium stores: mechanism for hereditary arrhythmia. *Proc Natl Acad Sci U S A* **100**, 11759–11764.

Valle G, Galla D, Nori A, Priori SG, Gyorke S, de Filippis V & Volpe P (2008). Catecholaminergic polymorphic ventricular tachycardia-related mutations R33Q and L167H alter calcium sensitivity of human cardiac calsequestrin. *Biochem J* **413**, 291–303.

Wade, RC, Gabdoulline RR, Lademann SK & Lounnas V (1998). Electrostatic steering and ionic tethering in enzyme-ligand binding: insights from simulations. *Proc Natl Acad Sci U S A* **95**, 5942–5949.

Wang Y, Xu L, Duan H, Pasek DA, Eu JP & Meissner G (2006). Knocking down type 2 but not type 1 calsequestrin reduces calcium sequestration and release in C_2C_{12} skeletal muscle myotubes. *J Biol Chem* **281**, 15572–15581.

Wang ZM, Messi ML & Delbono O (1999). Patch-clamp recording of charge movement, Ca^{2+} current, and Ca^{2+} transients in adult skeletal muscle fibers. *Biophys J* **77**, 2709–2716.

Wang ZM, Tang S, Messi ML, Yang JJ & Delbono O (2012). Residual sarcoplasmic reticulum Ca^{2+} concentration after Ca^{2+} release in skeletal myofibers from young adult and old mice. *Pflugers Arch* **463**, 615–624.

Winegrad S (1965). Autoradiographic studies of intracellular calcium in frog skeletal muscle. *J Gen Physiol* **48**, 455–479.

Wu YC, Tucker T & Fettiplace R (1996). A theoretical study of calcium microdomains in turtle hair cells. *Biophys J* **71**, 2256–2275.

Zhou G-Q & Zhong W-Z (2005). Diffusion-controlled reactions of enzymes. *Eur J Biochem* **128**, 383–387.

Zima AV, Bovo E, Bers DM & Blatter LA (2010). Ca^{2+} spark-dependent and -independent sarcoplasmic reticulum Ca^{2+} leak in normal and failing rabbit ventricular myocytes. *J Physiol* **588**, 4743–4757.

Ziman AP, Ward CW, Rodney GG, Lederer WJ & Bloch RJ (2010). Quantitative measurement of Ca^{2+} in the sarcoplasmic reticulum lumen of mammalian skeletal muscle. *Biophys J* **99**, 2705–2714.

Author contributions

CM planned and executed experiments, and contributed to data analysis and writing. MS carried out most experiments using biosensors, and contributed to data analysis and writing. LF contributed to the design, and assisted with execution of experiments, analysis and writing. PDA contributed to experimental design, analysis and writing, and developed the Casq null mouse. ER designed the study, helped with experiments, and contributed interpretation of results, data analysis and writing. All authors approved the final version for publication. The experiments were carried out at Rush University, Chicago.

Acknowledgements

We are grateful to ChulHee Kang for allowing the use of data published by his group in our Fig. 7, as well as for generous sharing of his ideas about roles and mechanisms of calsequestrin, to Bruno Allard, Andrew Ziman and Christopher Ward for help in implementing the fluo-5N measurement of $[Ca^{2+}]_{SR}$, and to Gustavo Brum for suggestions on the manuscript. This work was supported by grants from the National Institute of Arthritis and Musculoskeletal and Skin Diseases (AR049184 and AR032808 to E.R., and AR044750 and AR043140 to P.D.A.).

Author's present address

M. Sztretye: Department of Physiology, University of Debrecen, H-4012 Debrecen, Hungary.